GEOTECHNICAL ENGINEERING

LUNAR SURFACE ENGINEERING PROPERTIES EXPERIMENT DEFINITION

FINAL REPORT: VOLUME III OF IV
BOREHOLE PROBES

by

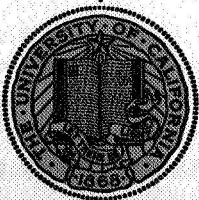R. E. GOODMAN
K. DROZD
S. CHIRAPUNTU
H. J. HOVLAND
T. K. VAN

JULY 1971

SPACE SCIENCES LABORATORY

UNIVERSITY OF CALIFORNIA · BERKELEY

Space Sciences Laboratory
University of California
Berkeley, California 94720

LUNAR SURFACE ENGINEERING PROPERTIES EXPERIMENT DEFINITION

FINAL REPORT: VOLUME III OF IV

BOREHOLE PROBES

By

R. E. Goodman
K. Drozd
S. Chirapuntu
H. J. Hovland
T. K. Van

PREFACE

This report presents the results of studies conducted during the
period July 19, 1969 — July 19, 1970, under NASA Research Contract
NAS 8-21432, "Lunar Surface Engineering Properties Experiment Definition."
This study was sponsored by the Lunar Exploration Office, NASA Head-
quarters, and was under the technical cognizance of Dr. N. C. Costes,
Space Science Laboratory, George C. Marshall Space Flight Center.

The report reflects the combined effort of five faculty investiga-
tors, a research engineer, a project manager, and eight graduate research
assistants, representing several engineering and scientific disciplines
pertinent to the study of lunar surface material properties. James K.
Mitchell, Professor of Civil Engineering, served as Principal Investigator
and was responsible for those phases of the work concerned with problems
relating to the engineering properties of lunar soils and lunar soil
mechanics. Co-investigators were William N. Houston, Assistant Professor
of Civil Engineering, who was concerned with problems relating to the
engineering properties of lunar soils; Richard E. Goodman, Associate
Professor of Geological Engineering, who was concerned with the engineer-
ing geology and rock mechanics aspects of the lunar surface; Paul A.
Witherspoon, Professor of Geological Engineering, who was concerned with
fluid conductivity of lunar surface materials in general; Franklin C.
Hurlbut, Professor of Aeronautical Science, who was concerned with
experimental studies on fluid conductivity of lunar surface materials;
and D. Roger Willis, Associate Professor of Aeronautical Science, who
conducted theoretical studies on fluid conductivity of lunar surface
materials. Dr. Karel Drozd, Assistant Research Engineer, performed
laboratory tests and analyses pertinent to the development of a borehole
jack for determination of the in situ characteristics of lunar soils
and rocks; he also helped in the design of the borehole jack. H. Turan
Durgunoglu, H. John Hovland, Laith I. Namiq, Parabaronen Raghuraman,
James B. Thompson, Donald D. Treadwell, C. Robert Jih, Suphon Chirapuntu,
and Tran K. Van served as Graduate Research Assistants and carried
out many of the studies leading to the results presented in this

report. Ted S. Vinson, Research Engineer, served as project manager
until May 1970, and contributed to studies concerned with lunar soil
stabilization. H. John Hovland served as project manager after May
1970, and contributed to studies concerned with soil property evaluation
from lunar boulder tracks.

Ultimate objectives of this project were:

1) Assessment of lunar soil and rock property data using information
   obtained from Lunar Orbiter, Surveyor, and Apollo missions.

2) Recommendation of both simple and sophisticated in situ testing
   techniques that would allow determination of engineering
   properties of lunar surface materials.

3) Determination of the influence of variations in lunar surface
   conditions on the performance parameters of a lunar roving
   vehicle.

4) Development of simple means for determining the fluid
   conductivity properties of lunar surface materials.

5) Development of stabilization techniques for use in loose,
   unconsolidated lunar surface materials to improve the
   performance of such materials in lunar engineering application.

The scope of specific studies conducted in satisfaction of these objectives
is indicated by the following list of contents from the Detailed Final
Report which is presented in four volumes. The names of the investigators
associated with each phase of the work are indicated.

VOLUME I

MECHANICS, PROPERTIES, AND STABILIZATION OF LUNAR SOILS

VOLUME II

MECHANICS OF ROLLING SPHERE-SOIL SLOPE INTERACTION
H. J. Hovland and J. K. Mitchell

VOLUME III

BOREHOLE PROBES

VOLUME IV

FLUID CONDUCTIVITY OF LUNAR SURFACE MATERIALS

VOLUME III
CONTENTS

Page

VOLUME III

Borehole Probes

Chapter 1. SUMMARY OF PREVIOUS WORK

R. E. Goodman, T. K. Van, and K. Drozd

INTRODUCTION

Instruments in boreholes capable of measuring adjacent rock and soil
deformation properties include: (a) penetrometers, which uniaxially load
small areas of the borehole walls to a high intensity; (b) dilatometers,
which expand a balloon inside the hole to radially load all of a section
of the wall; and (c) borehole jacks, which essentially conduct a plate
bearing test across opposing wall areas. Figure 1-1 shows an instrument
of the latter type which is currently being used in engineering practice.

Previous research explored the applicability of some of these
devices to lunar borehole testing and, in particular, examined the use
of such instruments to assess the strength of soils and rocks. Special
attention was given to borehole jacks for this purpose. Analytical work
employed finite element analysis, the theory of plasticity, and the
theory of elasticity using the complex variable method. A number of
solutions were reached for tractable sub-problems in the set of problems
posed when a jack is used to expand sectors of a borehole. In addition,
an investigation with physical models was made to explore the modes of
behavior for varying boundary conditions and materials, including both
elastic and plastic media. These investigations were reported by
Goodman et al. (Final Report of NASA Contract NAS 8-21432, Jan. 1970).
A brief review of these investigations follows.

REVIEW OF PHYSICAL MODEL STUDIES

Model studies were conducted in the laboratory using a model borehole
jack inside the central hole of plates of simulated rock. The jack consisted
of a hydraulic cylinder and sets of bearing plates of four different sizes.
Thus, it was possible to study the influence of the relative plate
dimensions on the modes of deformation and failure. Displacements across
the expanding jack were measured precisely as the hydraulic cylinder was
expanded inside the borehole. The fundamental data from the tests were
the jack load borehole deformation curves, and the observed deformations
and cracks of the model.
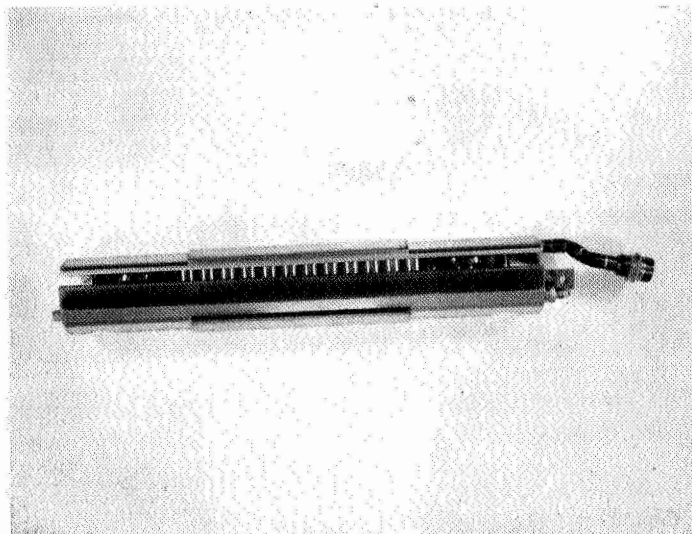
Fig. 1-1a. NX borehole jack (Goodman jack).
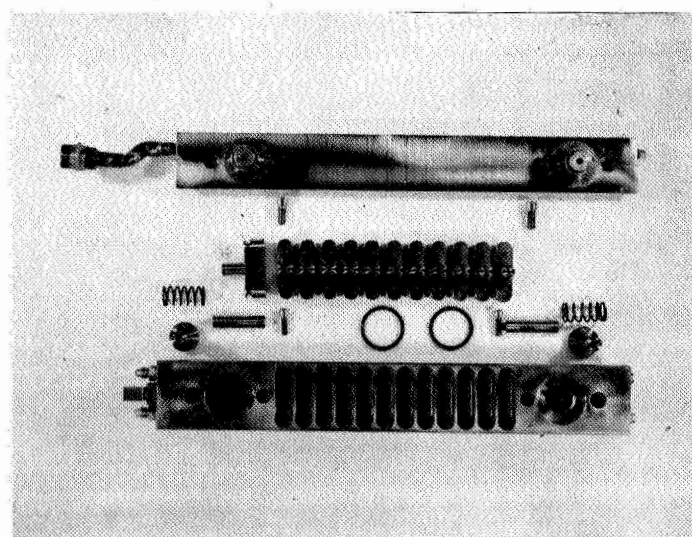
Fig. 1-1b. Structure of the NX borehole jack.

The results of the testing program reiterated the ability of the borehole jack method to determine deformability properties of soils and rocks. On the basis of the results, further study appeared to be warranted to determine strength properties for rocks. This is the subject of the next chapter. Determining strength properties for soils from borehole jack tests proved more difficult, since the main failure mode in the jack tests was punching whereas shearing is more common in most soil mechanics design problems. On the other hand, according to the results, "strength" values defined by a limiting deformation can be derived from borehole tests. Thus, borehole jack measurements for soils would be appropriate for limit design aspects of such problems as bearing capacity and safe wheel loadings where sinkage limits must be established.

On the basis of the model test results, a new borehole jack device was proposed for use in 2-inch lunar boreholes. The proposed jack was built and tested in the lunar soil simulant, as reported in Chapter 3 of this volume.

REVIEW OF THE THEORETICAL BASIS FOR DETERMINING THE STRENGTH
AND DEFORMABILITY OF ROCK BY BOREHOLE JACK MEASUREMENTS

A borehole jack forces two curved bearing plates against opposing sectors of the walls of a circular opening (Fig. 1-2), causing the walls to deform and eventually to fail. Brittle and initially unfractured materials fail in tension when the tensile strength of the borehole is reached; i.e., when $T_B = \sigma_{min}$, where T_B is the borehole tensile strength, and σ_{min} is the minimum principal stress (compression positive).

The stress σ_{min} is a function of the in situ stress field and the circumferential stress, σ_θ, induced along the circular boundary by borehole jack loading. Once σ_{min} has been determined, expressions can be derived which relate the borehole tensile strength, the in situ stress field, and the failure jack load to each other.

The circumferential stress, σ_θ, is a function of the applied load P and the manner in which this load is distributed over the contact surfaces between the bearing plates and the borehole walls.

The actual contact stress distribution is unknown. However, two types of boundary stress distributions were obtained, based on two different
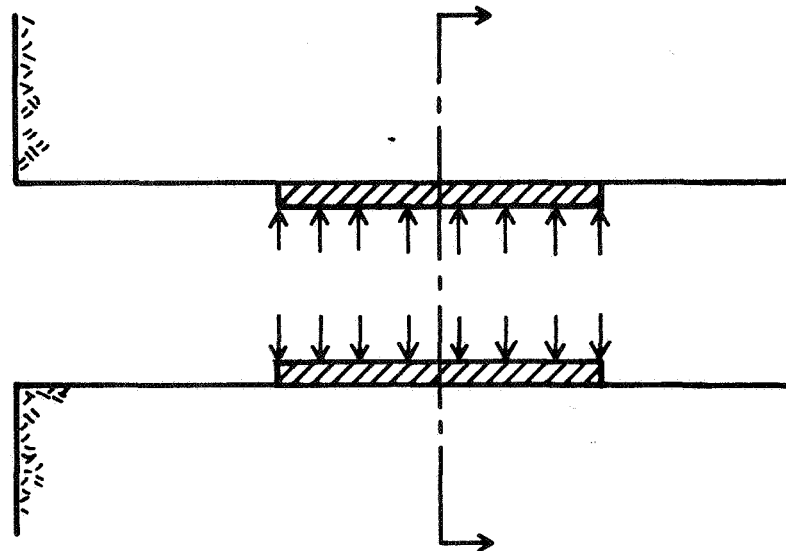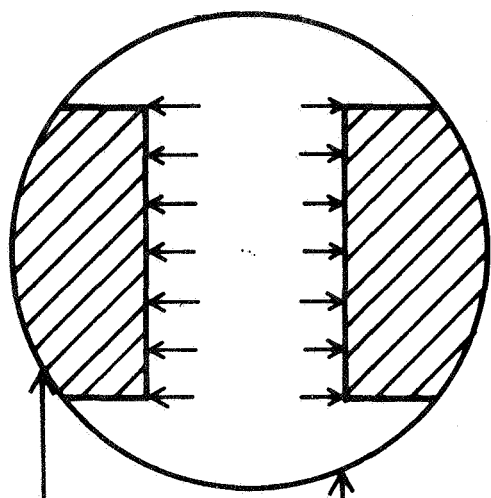
top view

bearing plate

borehole wall

side view

Fig. 1-2. Borehole jack loading.

physical considerations. Both distributions possess normal and shear components, each varying along the contact surfaces.

When the modulus of rigidity of the steel bearing plates is much greater than the modulus of the rock substance, the displacement over the contact surface is close to being uniform (Fig. 1-3a). This boundary displacement can be replaced by an equivalent boundary stress distribution to simplify the mixed boundary condition (along the unloaded boundary, the displacement varies). A uniform applied boundary displacement induces a contact stress distribution as shown in Figure 1-3b (Problem I), providing that the medium is linearly elastic and there is no slippage along the contact surfaces. Such a stress distribution can be approximated by the following equations (Van and Goodman, 1970):

$$\sigma_y = 0 \text{ and}$$

along the loaded areas,

$$\sigma_x = q\{k-(k-s) \cos \frac{\pi\theta}{2\beta}\} \quad ; \tag{1-1}$$

while along the unloaded areas,

$$\sigma_x = 0,$$

where: σ_x, σ_y = x- and y-components of the applied boundary stresses

q = stress σ_x at the center of the bearing plates

k = shape factor for the boundary stress distribution curve

2β = bearing plate central angle (see Fig. 1-3a).

From the theory of elasticity, the shear stress component along the contact surface is proportional to the differential displacement. Consequently, from the consideration of the differential displacement,
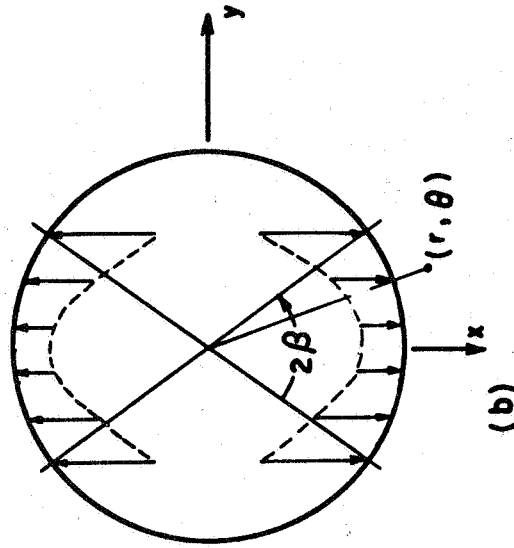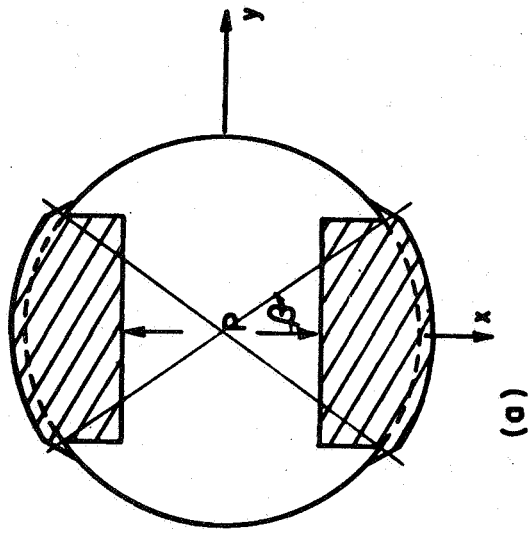
$$\sigma_x = q\{k - (k - s) \cos \frac{\pi\theta}{2\beta}$$

Fig. 1-3a. The mixed boundary conditions for rigid plate displacement problem.

Fig. 1-3b. The unidirectional contact stress distribution resulting from rigid plate displacement. (Problem I).

the appropriate contact stress distribution possesses a shear component, which varies along the contact surfaces in the same way as the differential displacement. One possible assumption for the contact stress state is that it is a uniaxial, unidirectional *principal* stress all along the contact surface. This assumption requires a shear stress to act along the boundary to satisfy the differential displacement consideration (Van and Goodman, 1970). The differential displacement along the contact surfaces is shown in Figure 1-4 (Problem II). The uniaxial principal contact stress distribution for Problem II is given by the following equations:

$$\sigma_y = \tau_{xy} = 0$$

Along the contact surface,

$$\sigma_x = q[k - (k-s) \cos \frac{\pi\theta}{2\beta}] \, , \quad \text{and} \tag{1-2}$$

outside loaded areas,

$$\sigma_x = 0 \, .$$

The stress component σ_x is a principal component because the shear component τ_{xy} is equal to zero at every point along the contact surfaces (Fig. 1-5).

From the solutions to Problem I and Problem II, the circumferential stress, σ_θ, along the circular boundary can be derived in terms of the boundary stress factor, k, as follows:

$$\sigma_\theta = K(k,\beta,\theta) \, \frac{P}{R} \, , \tag{1-3}$$

where

$K(k,\beta,\theta)$ = stress (concentration) factor, a function of the boundary stress factor k, the bearing plate width angle β, and the θ

P = total applied jack load/length of the bearing plates

R = radius of the borehole.
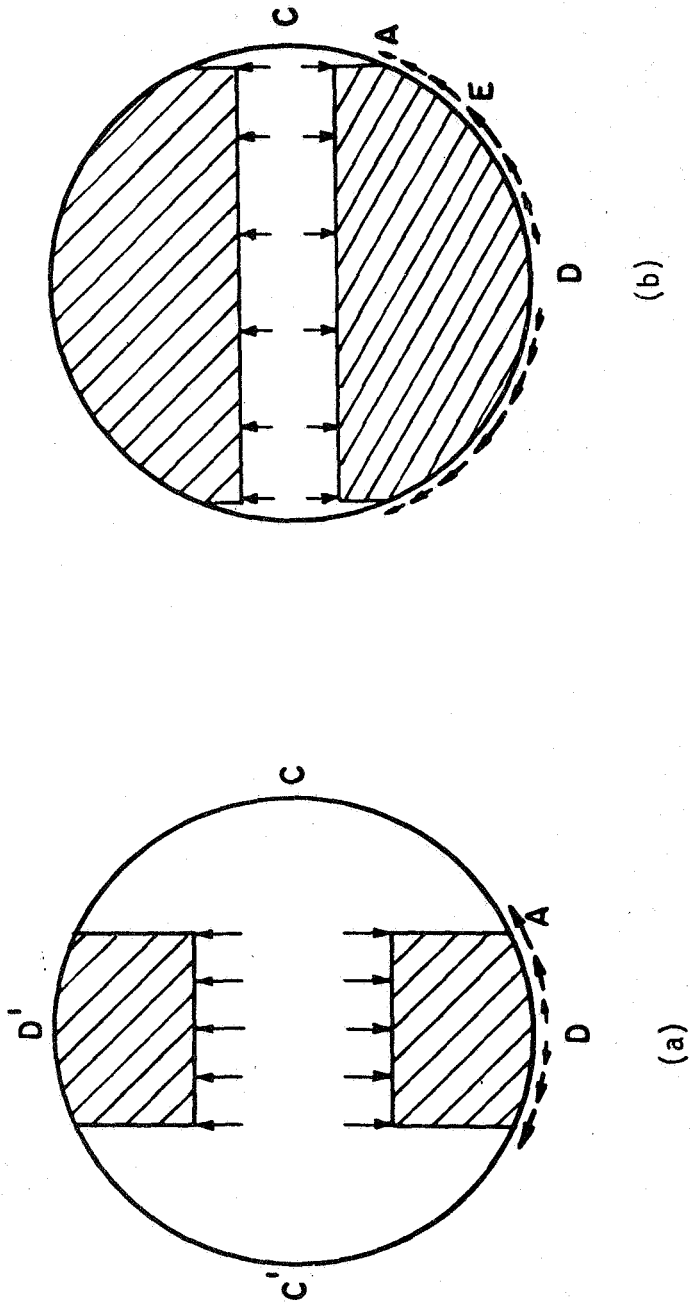
Fig. 1-4. Differential displacement along contact surfaces (Problem II).

(a)

(b)

$\tau_{xy} = 0$

(r, θ)

2β
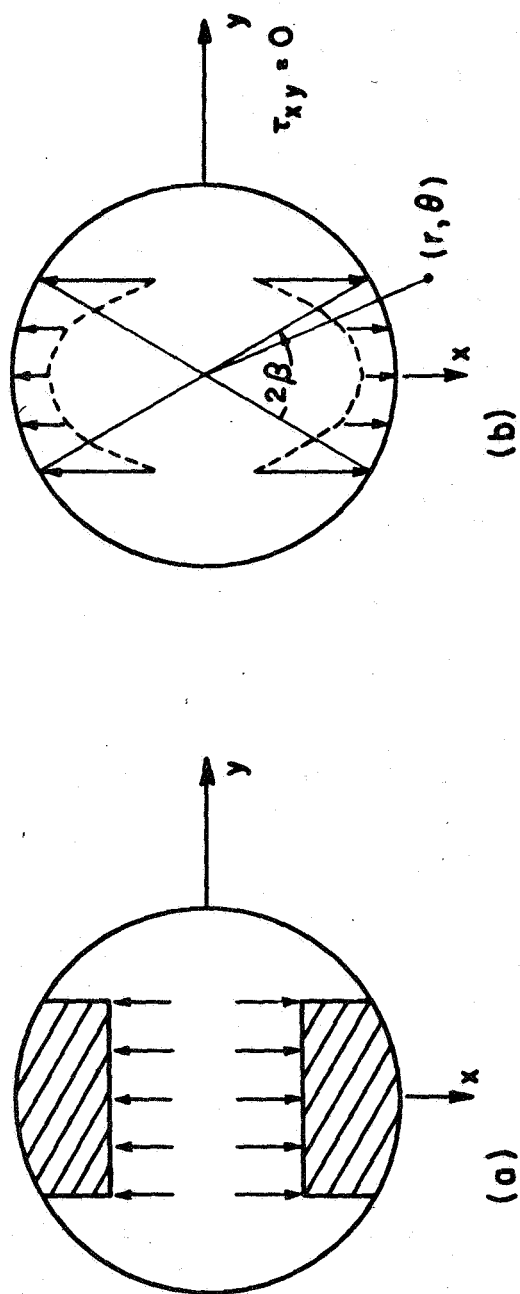
Fig. 1-5. a. Uniform unidirectional principal stress on bearing plates.
          b. Unidirectional principal stress along the contact surfaces.

The two boundary-value problems (Problems I and II) result in similar minor principal stress distributions, having the minimum value (i.e., the highest tensile stress) at the edges of the bearing plates. Consequently, either Solution I or Solution II can be used to interpret the results of borehole jack tests. However, the appropriate boundary stress distribution factors k for the two solutions are different.

A borehole jack with very narrow plates induces very high compressive stresses in the regions behind the contact surfaces; the material in these regions fails locally by one or more of the following modes: crushing, punching, and lateral chipping. Such a borehole jack acts as a penetrometer (Final Report NASA 8-21432, Jan. 1970).

When the bearing plates of the borehole jack are not very narrow, and the planes of weakness are absent, the borehole fails by tensile fracturing under jack loading.

The net stress distribution resulting from one isotropic in situ stress field and borehole jack loading has the highest tensile component at the four edges of the bearing plates; i.e., at $\theta = \pm\beta$, $\pi-\beta$, and $\pi+\beta$. Tensile fracturing is caused at these four points when the borehole tensile strength is reached:

$$T_B = K_T(k,\beta) \cdot \frac{P_F}{R} + 2p_1 \quad , \tag{1-4}$$

where:

T_B = borehole tensile strength (dimensions of pressure)

p_1 = magnitude of the in situ stress field

P_F = failure jack load/length of bearing plates

$K_T(k,\beta)$ = the maximum tensile stress factor, corresponding to $\theta = \beta$

R = radius of the borehole.

When the in situ stress field is biaxial (Fig. 1-6), with principal components $p_1 > p_2$, the net circumferential stress σ_θ is given by the
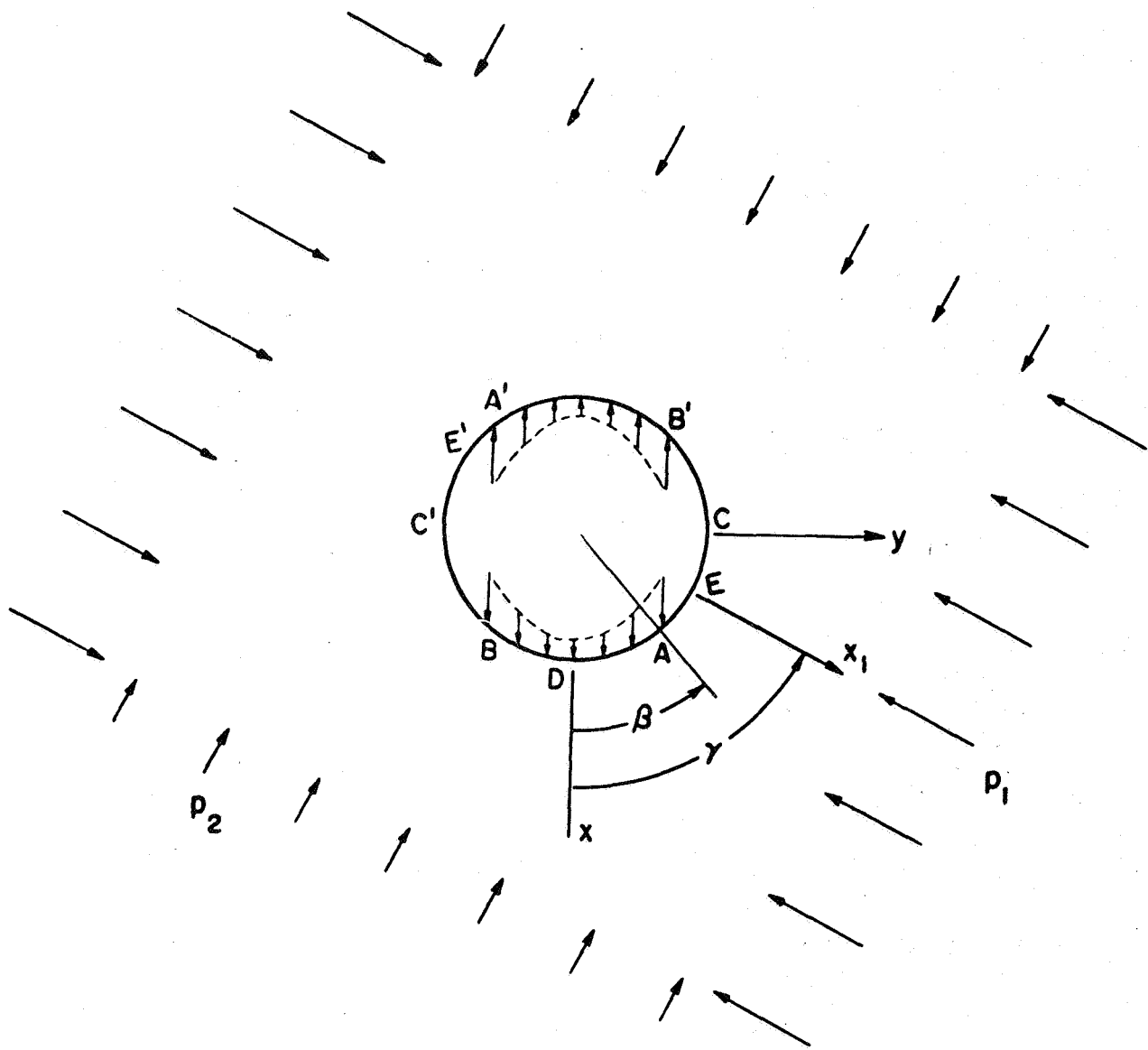
Fig. 1-6. Borehole jack loading in a medium initially under a biaxial in situ stress field.

following equation:

$$\sigma_\theta = p_1 + p_2 - 2(p_1 - p_2) \cos 2(\theta-\alpha) + K(k,\beta,\theta) \frac{P}{R} \quad . \qquad (1\text{-}5)$$

Knowing the stress σ_θ, the minor principal stress at every point along the boundary can be calculated. The minimization of this principal stress gives a relationship between the in situ stress field (principal components p_1 and p_2, and the orientation α), the borehole strength, and the failure load (Final Report NAS 8-21432, Jan. 1970).

Under normal field conditions, the in situ stress field usually induces a varying compressive stress component, σ_θ, along a circular opening, when $-p_1 + 3p_2 > 0$. Under certain conditions, there is a possibility that the induced stress, σ_θ, is tensile, when $-p_1 + 3p_2 < 0$. However, the tensile stress σ_θ is usually much smaller than the borehole tensile strength of the rock substance; that is, $|-p_1 + 3p_2| < |T_B|$. For these field conditions, the net stress distribution has the minimum minor principal stress (i.e., the most tensile) at two edges A and A' of the bearing plates (Fig. 1-6) where tensile fracturing takes place. The jack load to cause the fracturing is given by the following relation:

$$T_B = p_1 + p_2 - 2(p_1 - p_2) \cos 2(\beta-\alpha) + K_T (k,\beta) \frac{P_F}{R} , \qquad (1\text{-}6)$$

where

p_1, p_2 = principal stress components of the in situ stress field

α = the angle between the direction of jack loading and p_1 direction (Fig. 1-6).

There are three special jack orientations that give simplified relationships. When the jack is oriented so that one edge of a bearing plate is on the p_1 axis (i.e., $\alpha = \pm\beta$), Equation (1-6) becomes:

$$T_B = -p_1 + 3p_2 + K_T(k,\beta) \frac{P_F}{R} \quad . \qquad (1\text{-}7)$$

The rotation of the jack through an angle of 90 degrees from the previous orientation places one edge of a bearing plate on the p_2 axis. Then Equation (1-6) becomes

$$T_B = 3p_1 - p_2 + K_T(k,\beta) \frac{P_F}{R} \quad . \tag{1-8}$$

When the borehole jack with the bearing plate angle $\beta = 45°$ is oriented such that $\alpha = 0$ or $\alpha = \pi/2$, the following equation is obtained:

$$T_B = p_1 + p_2 + K_T(k,\beta) \frac{P_F}{R} \quad . \tag{1-9}$$

The deformability of the wall rock or soil can be calculated from the plate pressure vs. displacement curve by the following equation (Heuzé, Goodman, and Bornstein, 1970):

$$E = K \frac{\Delta P}{\Delta d/d} \tag{1-10}$$

where

    E = modulus of deformability

    ΔP = increment of plate pressure

    Δd = corresponding increment of diameter change

    d = diameter of borehole

    K = a constant depending on Poisson's ratio and the jack plate width.

Values of K resulting from a no-tension solution were also reported by Heuzé, Goodman, and Bornstein, (1970). For a material where no tension can develop, such as soil, the value of K is about 1.5.

REFERENCES

Goodman, R. E., Drozd, K., and Heuzé, F. E., "Borehole Probes,"
Vol. III, Final Report NASA Contract NAS 8-21432, Jan. 1970,
Space Sciences Laboratory Series 11 Issue 12.

Heuzé, Goodman, and Bornstein, "Borehole Jack Tests in Jointed
Rock-Joint Perturbation and No Tension Finite Element Solution,"
Chapter 3, Vol. III, Final Report NASA Contract 8-21432,
Jan. 1970, Space Sciences Laboratory Series 11 Issue 12.

Van, T. K., and Goodman, R. E., Chapter I, Vol. III, Final Report
NASA Contract NAS 8-21432, Jan. 1970, Space Sciences Laboratory
Series 11 Issue 12.

Chapter 2. AN EXPERIMENTAL STUDY OF
THE MECHANISM OF FAILURE OF ROCKS UNDER BOREHOLE JACK LOADING

T. K. Van and R. E. Goodman

PURPOSE AND SCOPE OF THE EXPERIMENT

The theoretical aspects of the problem of borehole jack loading in rocks were presented by Van and Goodman, 1970, and were reviewed in Chapter 1 of this volume. This report is concerned mainly with experiments carried out on brittle materials to define the actual mode of failure, to check the validity of the theory presented, and to determine the two unknown parameters to be used with the theoretical solutions. The unknown parameters include the tensile strength T_B of the medium under the borehole jack loading and the boundary stress distribution factor, k, discussed in the next section. The tensile strengths of rock substances and brittle materials vary greatly with the mode of loading. The most commonly used are the uniaxial (direct) tension strength and flexural strength. It was suggested (Van, 1967) that the tensile strengths determined by the borehole jack test should be expressed in terms of the flexural strengths of the materials. The ratio between the borehole strenth, T_B, and the flexural strength, T_S, is denoted as the borehole strength ratio, L_r.

The jack load to cause fractures and the crack locations are controlled by a number of factors. These factors include the width of the bearing plates, the magnitude and orientation of the in situ stress fields, the borehole tensile strength of the rock medium, and the contact stress distribution. Once the borehole tensile strength of the medium is known, the appropriate boundary stress factors, k, (Van and Goodman, 1970) for the chosen stress distribution (Problem I or Problem II) can be determined.

Applied boundary stresses that are uniform in the longitudinal direction induce the same stress distribution in a linearly elastic medium, whether the medium is under plane strain or plane stress condition. Therefore, either condition can be used in our experimentation, until cracking begins. Most of the tests in the laboratory were under the plane stress condition, which was more easily arranged. An experimental borehole jack was built to apply uniaxial forces against the wall of a

circular opening. The description of this jack was given in detail in last year's final report (Van and Goodman, 1970).

Competent hard rocks such as granite are very close to being linearly elastic, while weak rocks such as sandstones are brittle but nonlinearly elastic. The testing with the experimental borehole jack was made on simulated materials, both linearly and nonlinearly elastic.

The problem of tensile failure by borehole jack loading is solved once the strength ratio, L_r, and the appropriate boundary stress distribution factors, k, have been determined. These two parameters are basically material properties.

The solution was used to interpret the test results from NX-borehole jack tests in the laboratory and a limited number of tests in the field.

BOREHOLE JACK EXPERIMENTS WITH SIMULATED ROCK MATERIALS

Experimental Borehole Jack and Testing Setup*

The experimental borehole jack was designed to apply a uniaxial load against the wall of a 3-inch cylindrical hole. The device consists mainly of a cylindrical hydraulic piston of 0.63-inch diameter. The piston has a maximum stroke of 1.27 inches. The hydraulic piston forces two symmetrical, curved bearing plates against the wall of the opening. Four different sets of bearing plates were built of hardened steel. Each plate is an arc of a 3-inch-diameter circle having a square groove with rounded corners, into which the hydraulic piston is fitted. The experimental jack under calibration and the general view of the plane strain testing set up are shown in Figure 2-1.

Most of the tests were under the plane stress condition. Some attempt was made to carry out the plane strain condition. A model plate was confined between two rigid guarding plates, tightened together by bolts; a hardened steel base plate (0.5-inch thick) and a top plate made of plexiglass (1.5 inches thick) were used. When jack load was applied,

---

*A detailed description of the jack and the problems involved in the testing of soils was given in Chapter 2 of last year's Final Report (Van and Goodman, Jan. 1970).
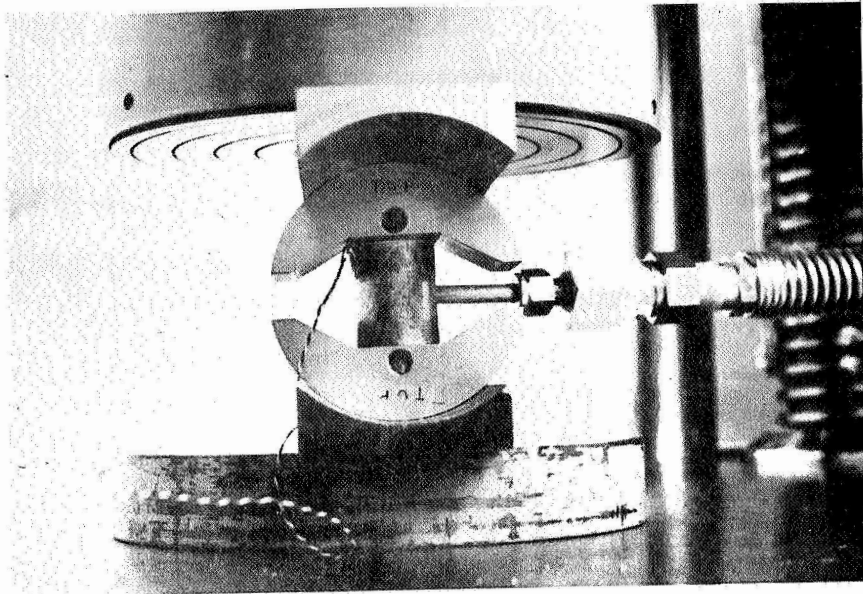
(a) The jack under calibration
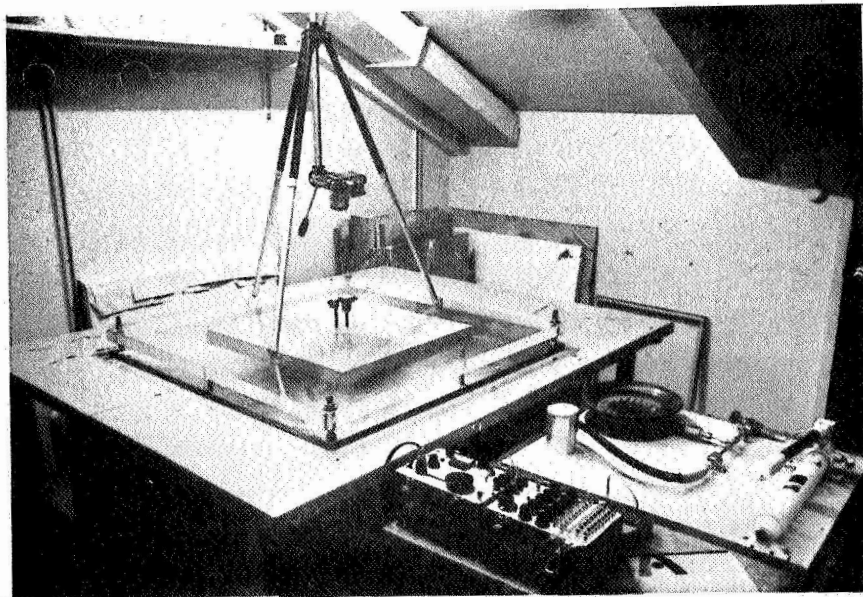
(b) The plane strain testing set up

Fig. 2-1. Experimental borehole jack.

the guarding plates were bent at the center by the induced vertical stress components. There were also the problems of friction and poor contact between the model plate and the guarding plates. All these problems were eliminated under the plane stress arrangement.

Simulated Brittle Materials and Model Plate Preparation

The materials used to simulate brittle media included:

1. Plaster of paris (U.S. Gypsum "Red Top")
2. Powdered diatomite (Johns Mansville "Celite")
3. Monobasic Sodium Phosphate, used as a retarder (Allied Chemical Co.)
4. Medium sand (PCA "Lapis Lustre" No. 20)
5. Portland cement (PCA type 1).

Plaster-celite material simulated fairly well a homogeneous isotropic brittle elastic medium. It was especially suitable for our experimentation because of its low tensile and compressive strengths. Concretes have been used to simulate rocks in the laboratory. They were used in the study of deformability measurement with a borehole jack (Van, 1967). Concrete mixtures are highly nonhomogeneous, nonisotropic, and not linearly elastic. A weak concrete was used to simulate a weak rock such as sandstone. The cement content was very low, less than 10 per cent by weight. Tensile fracturing took place in the cement matrix, around the sand grains.

The concrete model plates, 24 by 24 by 15 inches were cast in wooden frames set on flat horizontal platforms. The 3-inch-diameter opening was created by setting a cylindrical core at the frame center during the casting. To prevent sticking, the central core and the frame were painted with a release compound (Krylon's Silicon Spray-on "Powerfilm"). The model plates were cured at a constant temperature and at 100 per cent relative humidity for 1 week, then dried in open air at room temperature for 2 weeks. Cylinders 6 inches in diameter and 12 inches in height were cast for the determination of the mechanical properties.

Plaster-celite model plates were cast in aluminum molds set vertically. The plaster-celite and concrete model plates had the same dimensions. To have good castings, the following procedure was followed:

1. Celite was soaked in water and stirred until all the
    bubbles were removed;

2. Chemical retarder was added;

3. One-fifth of the plaster was added at steps 1 and 2; the
    mixture was stirred using a commercial mixer until all
    lumps were removed;

4. When the mixture started to thicken, it was poured into
    the aluminum mold. Water bleeding would occur when
    there was not enough mixing; this loss of water would
    greatly change the properties of the material.

The model plates were removed from the molds after 2 hours. The
plates were then continuously subjected to warm air currents produced by
electric heaters (125°F) for 20 days. The final moisture content of the
plates was 20 per cent by weight. Small cylinders were cast for the
determination of the mechanical properties.

The composition and properties of the simulated materials are given
in Table 2-1. Good control of the temperature and the air moisture must
be made during the curing of the model plates to insure the consistency
of their mechanical properties.

Test Results

As mentioned earlier, either plane strain or plane stress condition
can be used. To eliminate the problems of friction and poor contact
between the model plate and the guarding plates, as well as the bending
of the guarding plates, most of the tests were made under plane stress
condition. The test set up is shown in Figure 2-1b, with the top
plexiglass plate removed.

Load increments of 31.70 pounds (100-psi line pressure) were applied
with a hydraulic pump. Bearing plate displacements were read 1 minute
after each load application.

Microscopically, plaster-celite is highly porous. Failure by
punching was observed in all six tests on plaster-celite plates when
the narrowest bearing plates were used ($\beta = 10°$). The punching was
caused by the structural collapse of the micro-pores in the plaster-celite
material. The average compressive stress to cause the punching was found

Table 2-1. Composition and properties of the simulated materials.

Material	Composition	Proportion of content by weight	Tensile Strength		Compressive Strength (psi)	Modulus of Elasticity	Cohesion (psi)	Friction Angle (°)
			Brazilian (psi)	Flexural (psi)				
plaster-celite	plaster celite water retarder	100: 160: 40: 0.2	120	280	640	28×10^4	138	43
concrete	sand cement water	100: 5: 5	51	118	317	3.5×10^4	19.5	43

to be 24 per cent higher than the average compressive strength of the material. These results agree with the finding made earlier by Chercasov (1967).

The plaster-celite plates failed by tensile fracturing when wide bearing plates were used. Two cracks were formed at the edges of the edges of the bearing plates in 17 out of 24 tests. In three tests, the cracks occurred at the locations $\theta = \pi/2$ and $\theta = -(\pi/2)$. In 4 out of 24 tests, one crack was formed at an edge of a bearing plate; the second crack occurred at the location $\theta = \pi/2$. The cracking patterns are shown in Figure 2-2.

All the concrete model plates failed by tensile fracturing. As expected, the cracking took place in the cement matrix, going around the sand grains. In 13 out of 16 tests, the cracks were formed at the edges of the bearing plates. In two tests, the cracks occurred at the locations $\theta = \pi/2$ and $\theta = -(\pi/2)$. In one test, one crack occurred at an edge of a bearing plate; the second crack was formed at the location $\theta = \pi/2$.

The typical load-deformation curves for plaster-celite and concrete are shown in Figures 2-3a and 2-3b.

Tensile failure takes place when the borehole tensile strength of the material is reached. However, the fracture initiation takes place much earlier, when the flexural strength of the medium is reached (see discussion of the results). The jack loads which induce a maximum tensile stress equal to the flexural strength of the material are calculated from Equations (1-4) and (1-6) through (1-9), where T_B is replaced by T_S, and P_F is replaced by P_{init} (fracture initiation load).

The load-deformation curves were very close to straight lines. The splitting of the model plates took place instantaneously; i.e., no cracks were observed before the failure occurred.

The failure loads and the theoretically calculated crack initiation loads are compared in Figures 2-4 through 2-7.
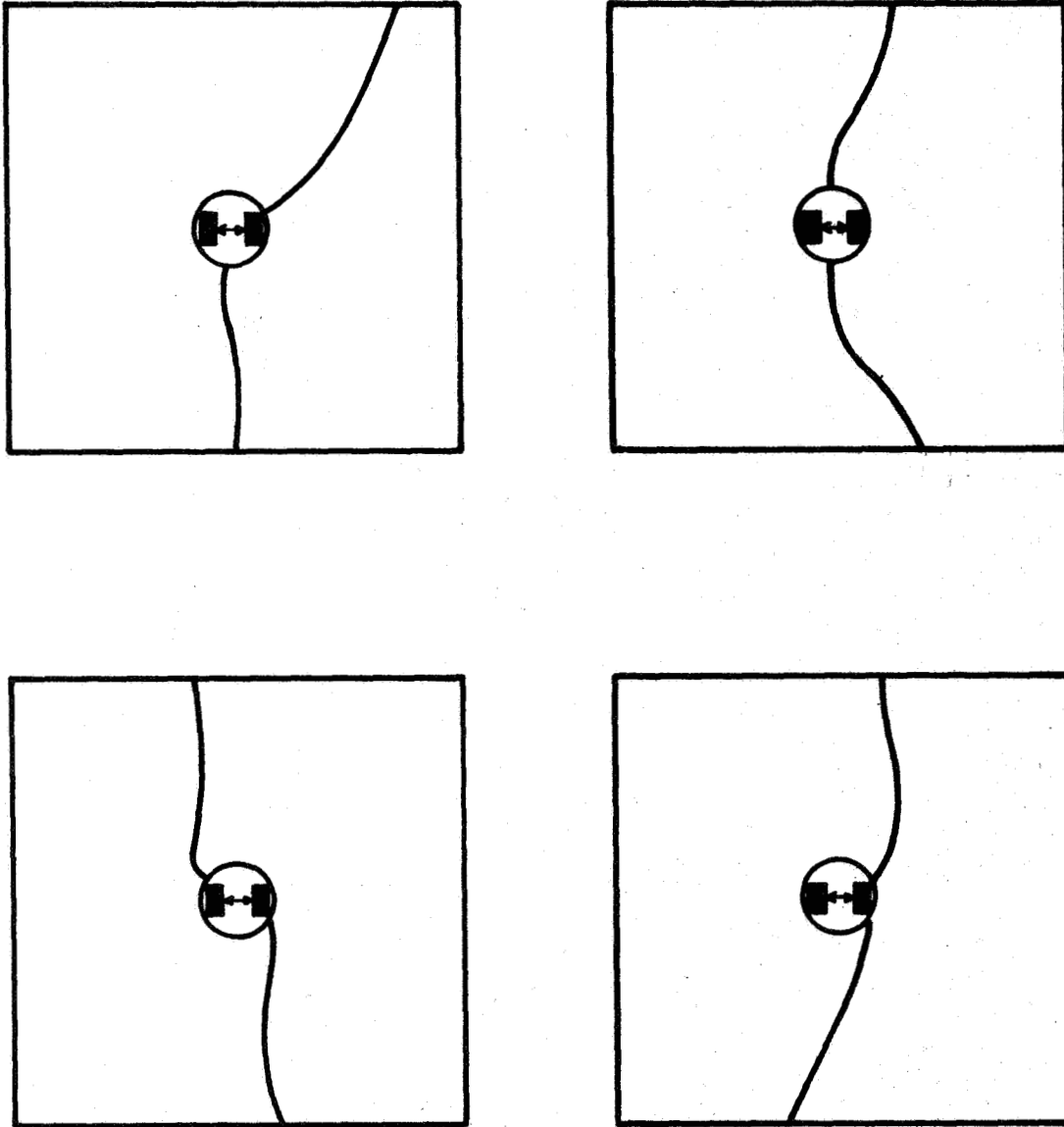
Fig. 2-2. Typical cracking patterns in concrete and plaster-
celite plates under borehole jack load.
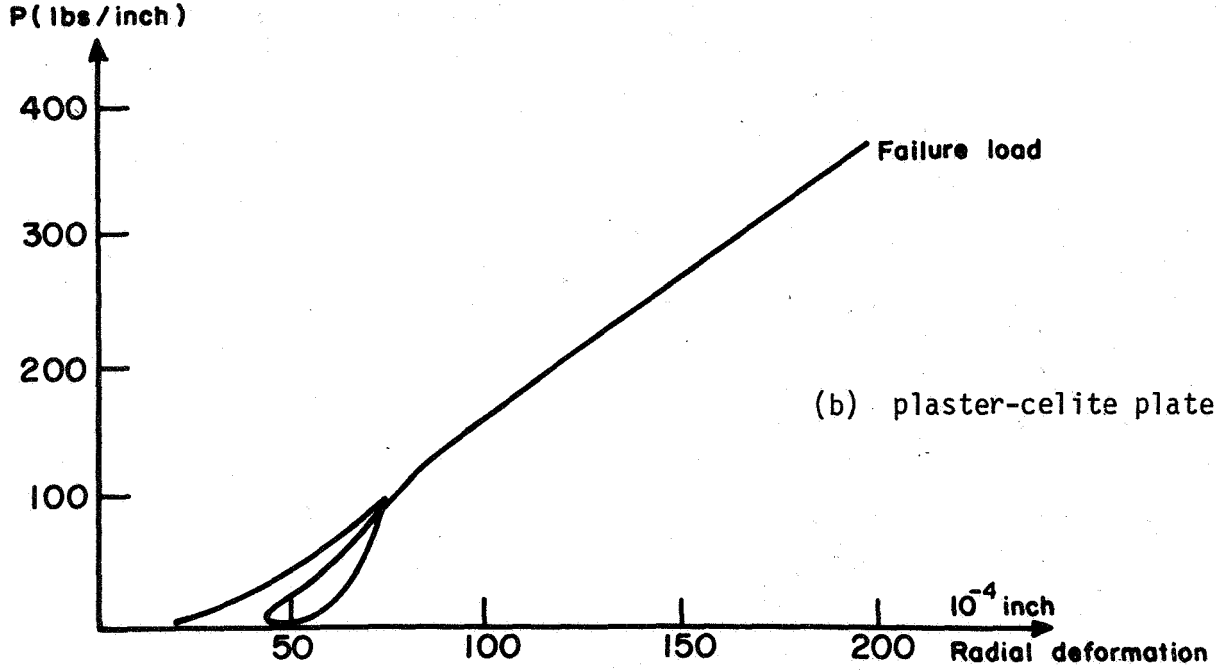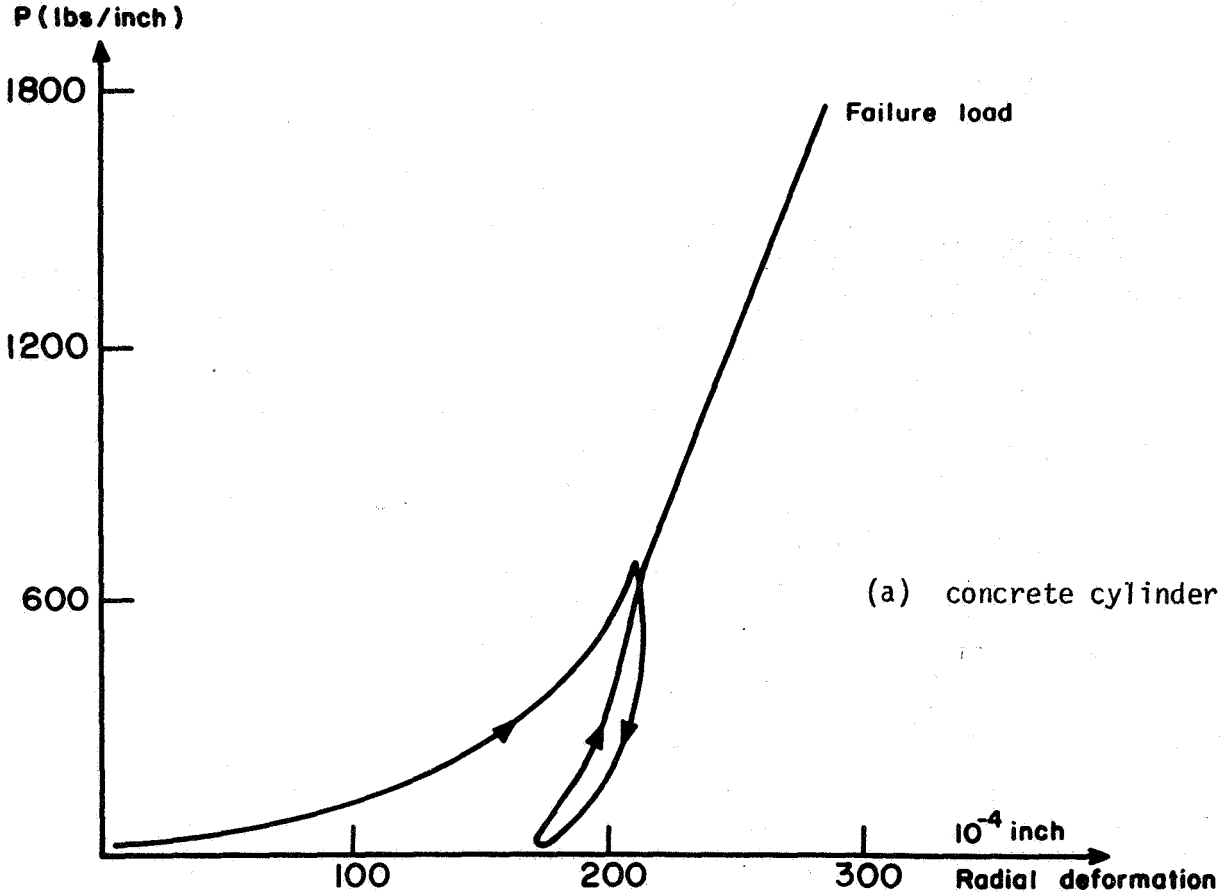
Fig. 2-3. Load-deformation curves.
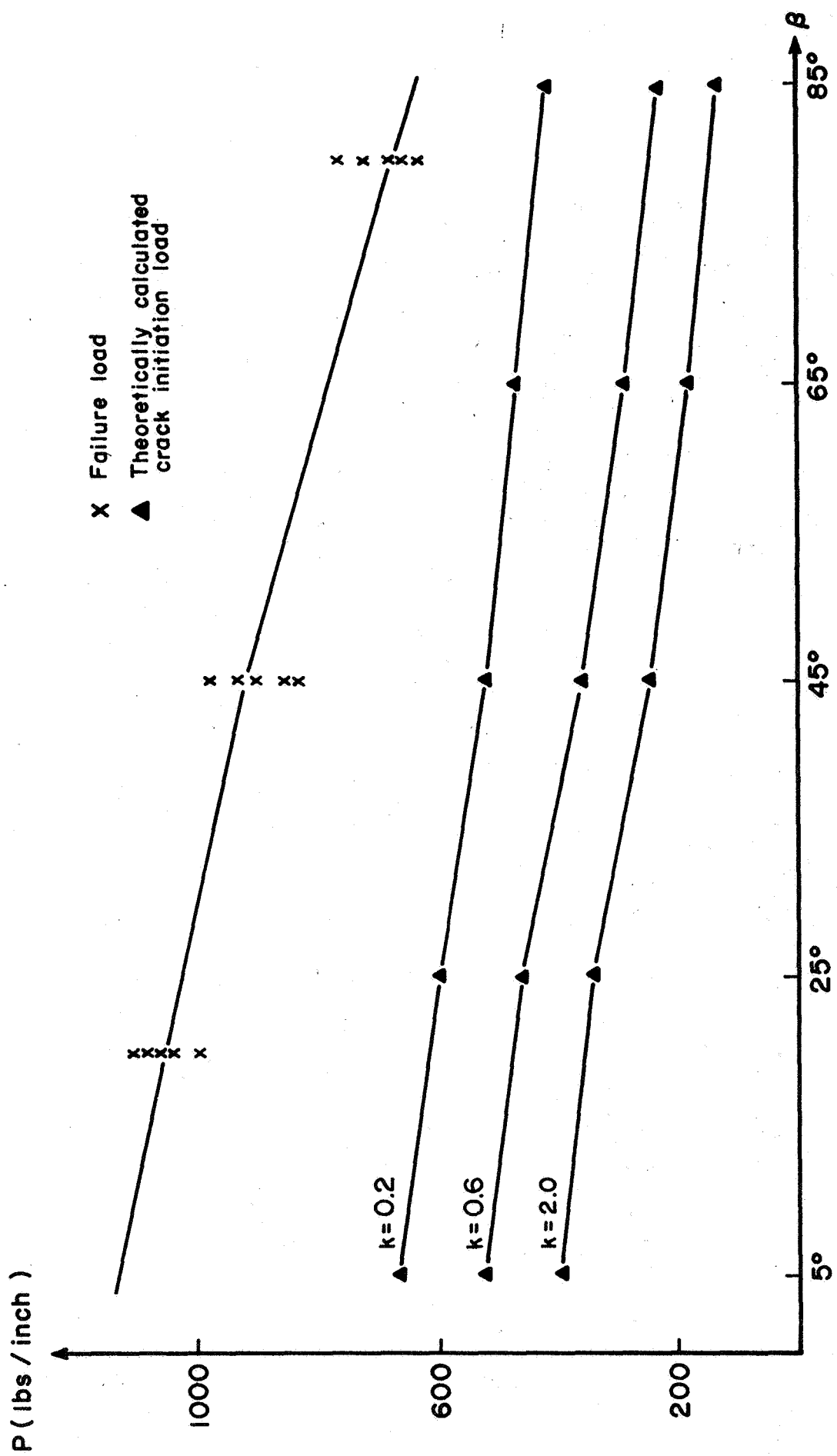
Fig. 2-4. Failure and crack initiation loads for plaster-celite (Solution I).
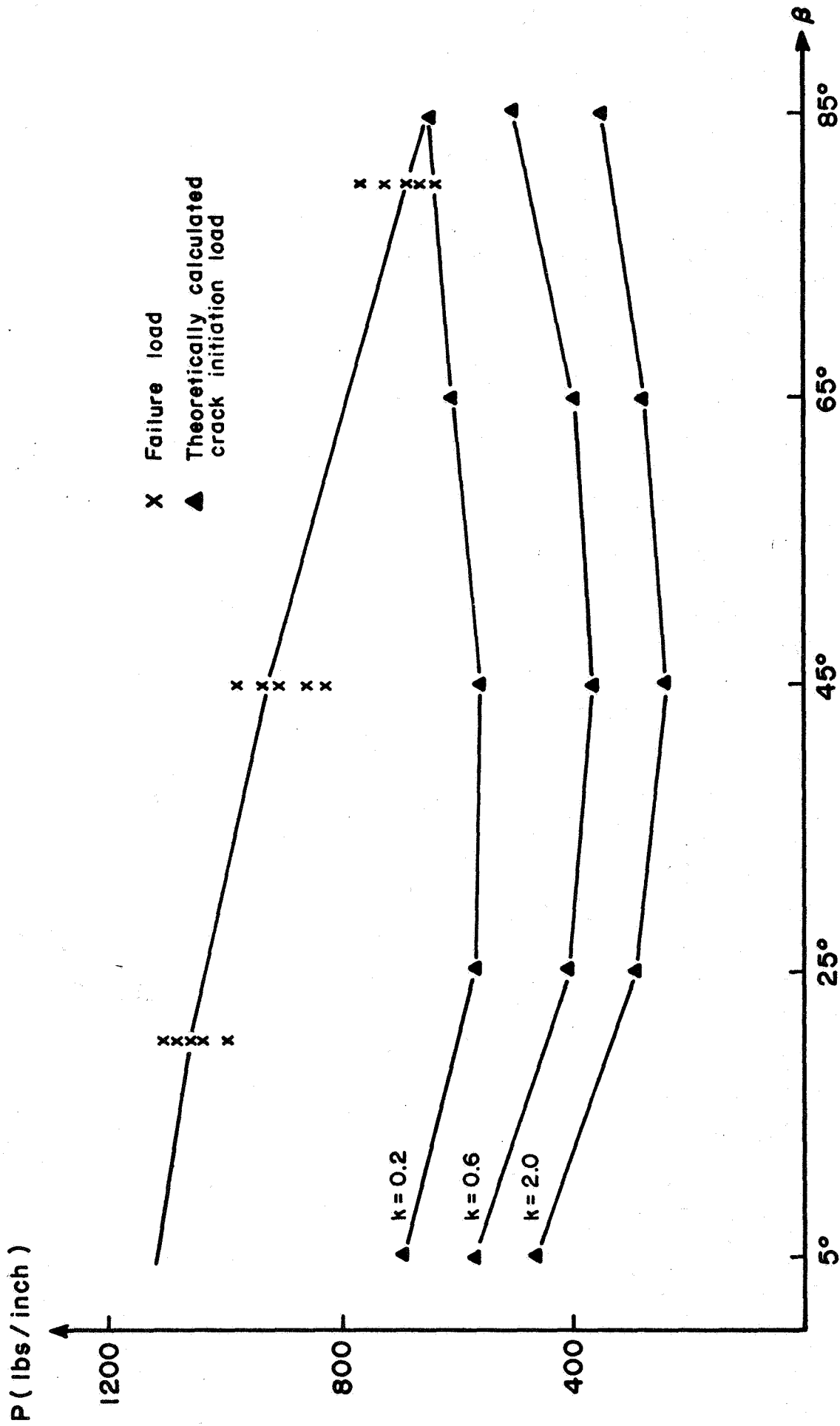
Fig. 2-5. Failure and crack initiation loads for plaster-celite (Solution II).
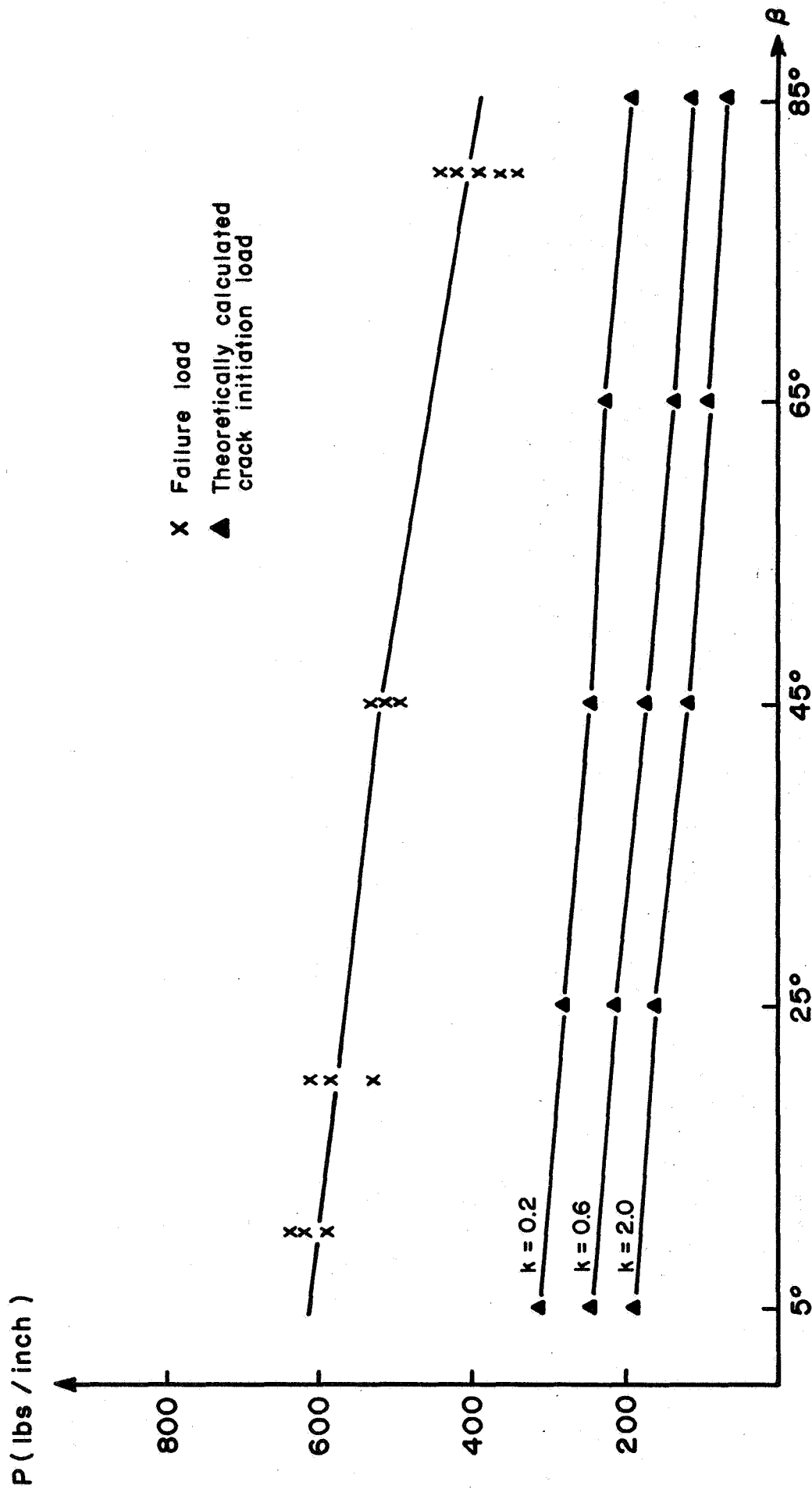
Fig. 2-6. Failure and crack initiation loads for concrete (Solution I).
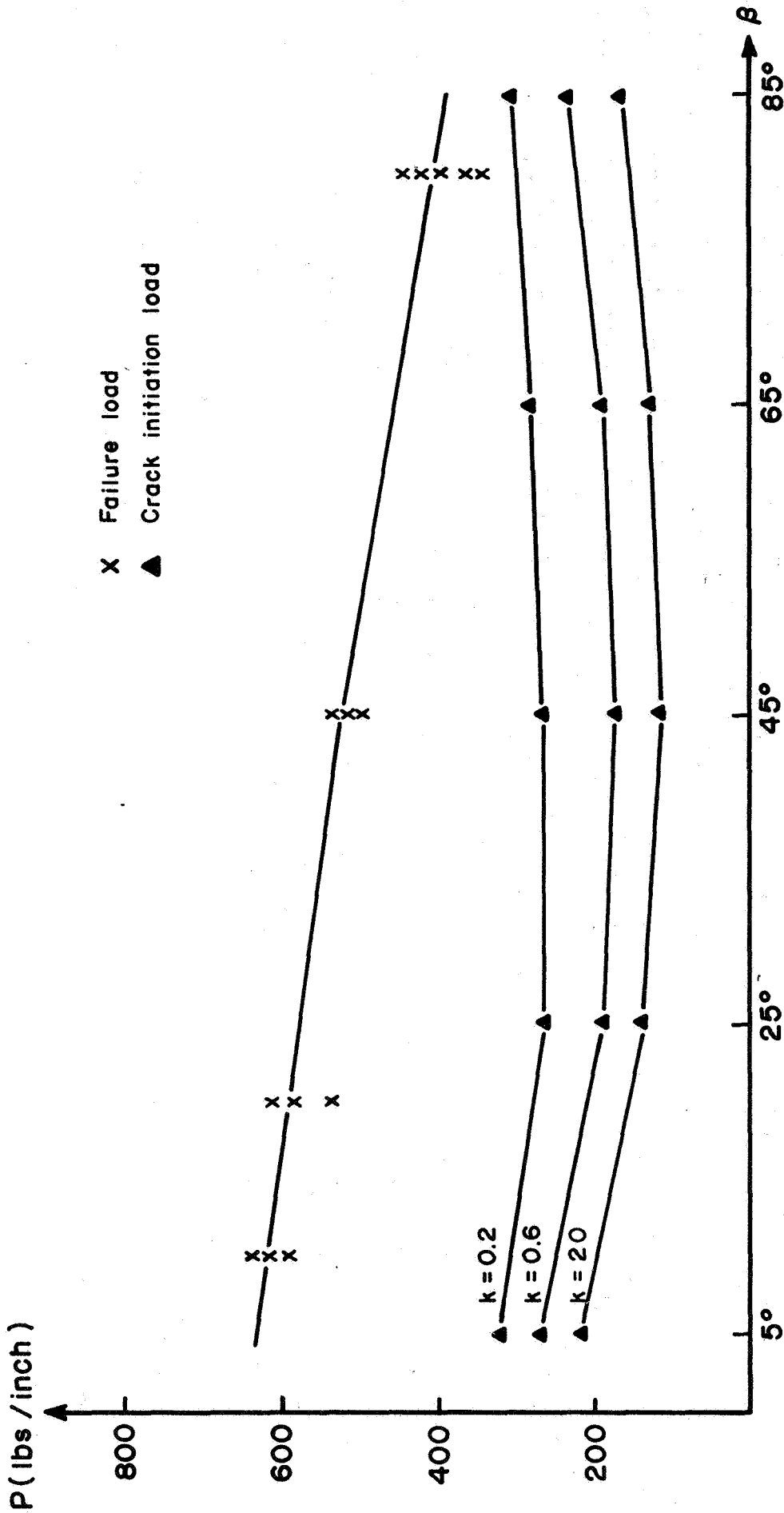
Fig. 2-7. Failure and crack initiation loads for concrete (Solution II).

Discussion of the Results

Location of the tensile cracks.

Elastic solutions to both Problem I and Problem II predict that the borehole jack loading induces highest tensile stresses at the edges of the bearing plates. Tensile fracturing should occur at these locations when the borehole tensile strength of the medium is reached.

From the testing of the simulated model plates, most of the cracks occurred very close to the edges of the bearing plates, in agreement with the theoretical prediction.

The location of most of the cracks confirms the existence of a significant shear stress component along the contact surfaces between the bearing plates and the walls of the opening. Therefore, the two previously proposed boundary stress distributions (Van and Goodman, 1970) are reasonable. The normal contact stress distributions, assumed by previous investigators (Absi and Seguin, 1967; Wyanecki, 1968), induce constant tensile stresses in the circumferential direction along the unloaded arcs. For these conditions, the tensile cracks would be formed simultaneously and at random at many points in the unloaded arcs.

The occurrence of some cracks at the locations $\theta = \pi/2$ and $-(\pi/2)$ can be explained by the actual behavior of the material around the opening during the loading. First, the borehole tensile strength of the material varies with confinement; the variation of T_B along the opening is shown in Figure 2-8. Secondly, real materials yield when they are subjected to large stresses; the yielding transfers some load from the highly stressed zones to the neighboring regions. The yielding at the edges of the bearing plates reduces the maximum tensile stress and shifts its location away from the nearest edge (Fig. 2-9). Thirdly, under loading, the opening deforms and becomes an "oval." This geometrical change of the boundary increases the tensile stress at the location $\theta = \pi/2$ and at the same time reduces the maximum tensile stress (Fig. 2-10).

The net tensile stress distribution curve changes its shape with the level of loading. When the stress curve and the strength curve touch each other, the tensile fracturing takes place. The two curves could
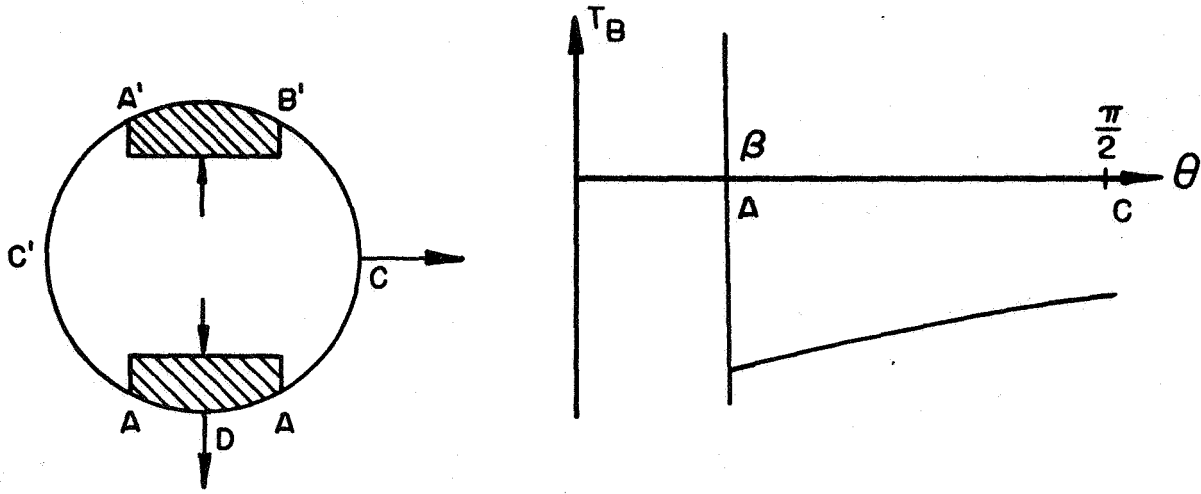
Fig. 2-8. The variation of the tensile strength along the boundary of the opening.
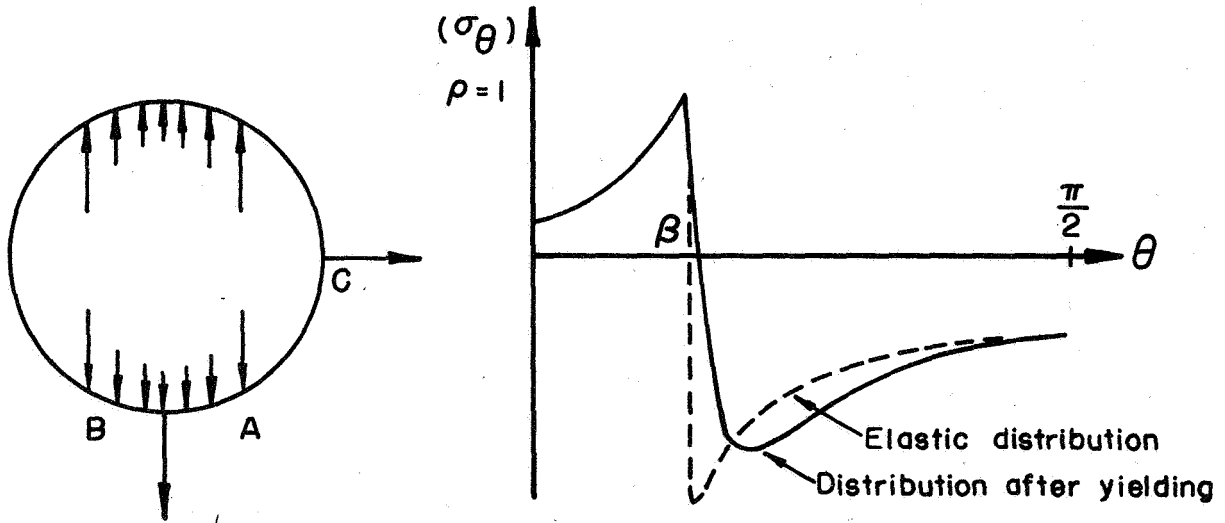
Fig. 2-9. The reduction of the maximum tensile stress and the shifting of its location due to yielding.
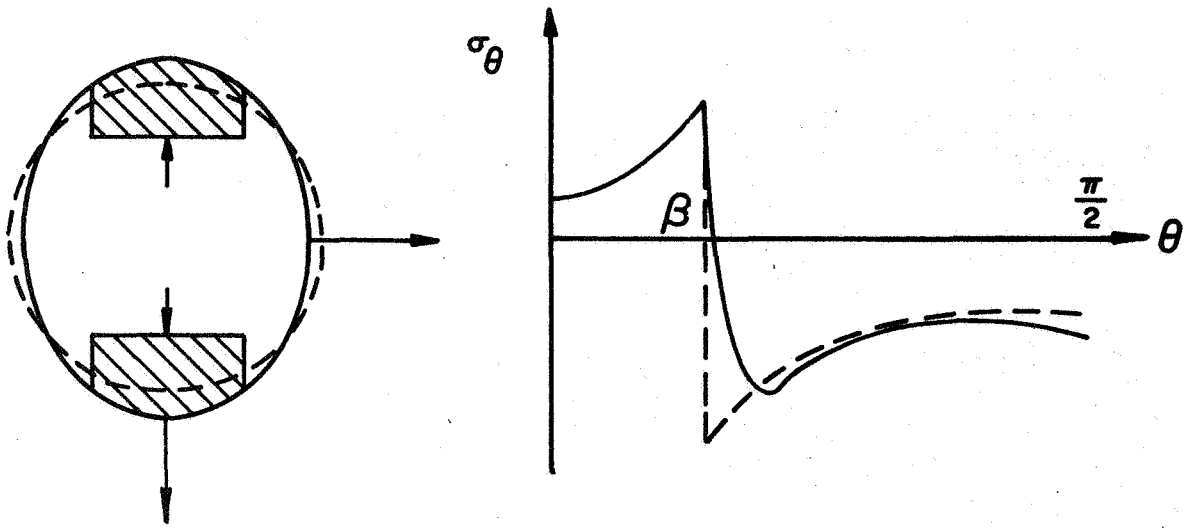
Fig. 2-10. The effect of the change in the shape of the opening on the distribution of the circumferential stress.
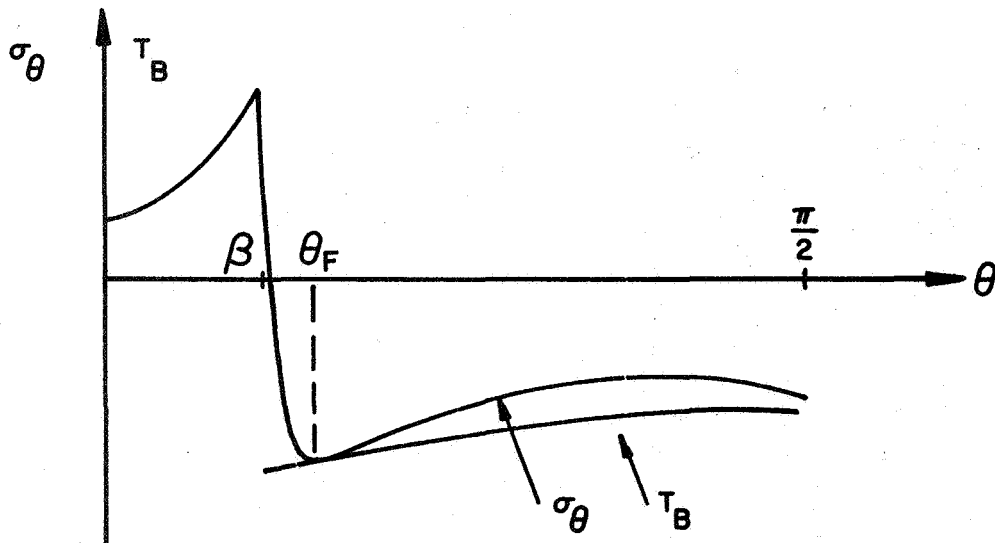
Fig. 2-11. The initiation of a crack close to an edge of the bearing plate.

touch either at θ β (that is, close to a bearing plate edge) at the location θ = π/2, or at both locations simultaneously (Figs. 2-11, 2-12, and 2-13).

Relationship between borehole tensile strength and flexural strength; and the borehole strength ratio.

The brittle failure of rocks and solids includes the initiation of fracture and the phase of fracture propagation. The phase of fracture propagation consists of an initial stable phase and an unstable phase in which the coalescence of small cracks brings on failure (Bianiawski, 1967). Crack initiation takes place when the criterion for fracture initiation is satisfied; however, a much larger load is required to induce the propagation of the fracturing. The ratio between the failure stress and the fracture initiation stress depends on the material and the mode of loading. In the studies of the brittle fracture of rocks, it has been found frequently that the failure load is much larger than the fracture initiation load; the ratio could be as much as three times (Bianiawski, 1967).

Under borehole jack loading, rocks fail by tensile fracturing. The tensile strength for this mode of loading is different from the well-known uniaxial, Brazilian (split tensile), and flexural strengths because the tensile depends on the mode of loading.

In direct tensile or uniaxial tests, the plane of failure is normal to the loading direction. Under direct tensile stress a specimen can fail anywhere along the length of the specimen; however, failure takes place only at the point of minimum tensile strength. In a Brazilian test, a cylindrical specimen is placed horizontally between the bearing plates of a testing machine and is loaded to failure by compression. In this test, a uniform tensile stress is developed along the vertical diametrical plane of the specimen; the failure is initiated at a point of minimum tensile strength on that plane. In a flexural test, either a cylindrical or a prismatic specimen is loaded in a three-point loading device to failure. The maximum tensile stress is developed at one point for a cylindrical specimen and along a line for a prismatic one. The crack initiation takes place at such a point or at a point along such a line.
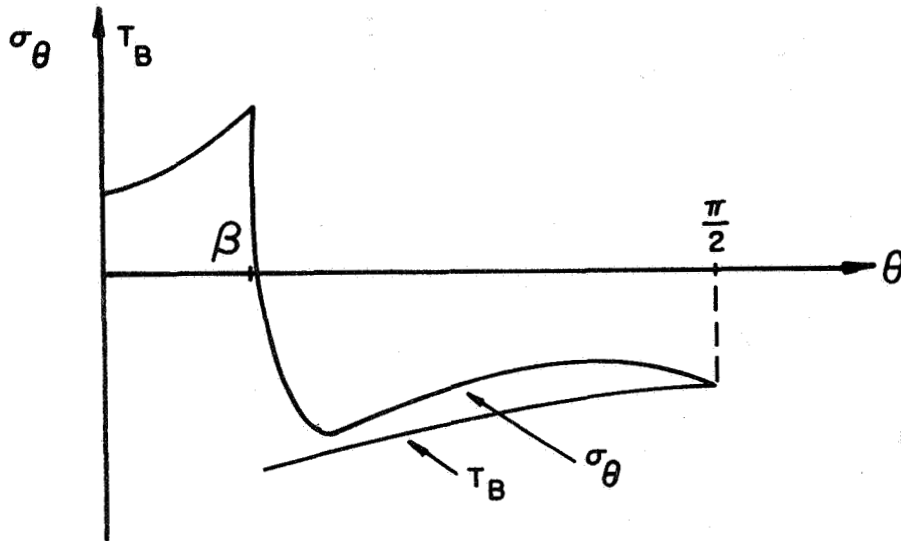
Fig. 2-12. The initiation of a crack at the location.
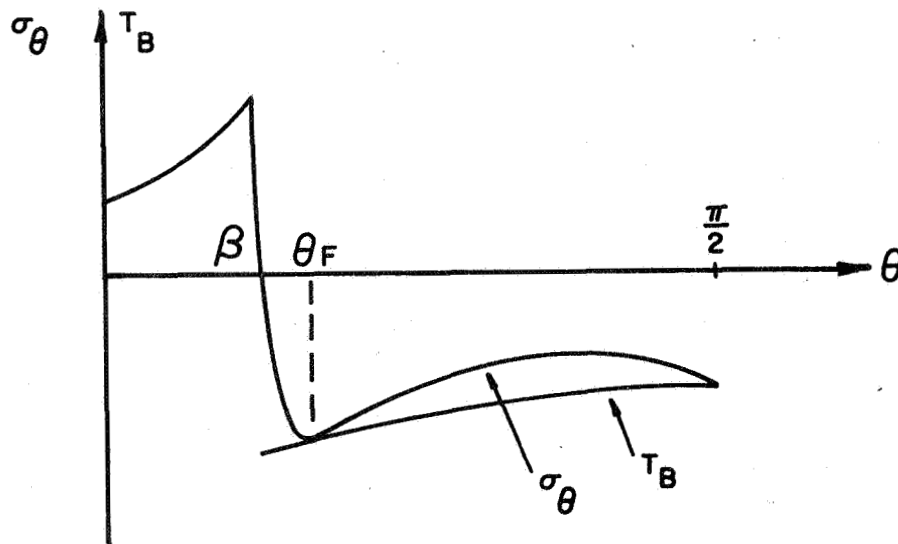
Fig. 2-13. The initiation of two cracks, one close to an edge
of a bearing plate and another at the location $\theta=\pi/2$.

The flexural strength is a measure of the outer fiber tensile strength of a material and is higher than either the direct tensile or the Brazilian strength. This higher value is presumed to result from the fact that only a small area on the opposite side of the specimen directly under the loading is subjected to the maxiumum tensile stress (or strain). Hence, the probability of a defect occurring in this small area is less than that of an equivalent defect occurring on the diametrical plane of a Brazilian specimen or in the length of a direct tensile specimen (Obert and Duvall, 1966).

Under borehole jack loading, maxiumum tensile stress is developed along four lines; i.e., the edges of the bearing plates. The probability of a defect occurring along these lines is about the same for an equivalent defect occurring in the small area in the flexural specimen mentioned above. Fracture initiation should take place at about the same maxiumum tensile stress for both modes of loading. In a flexural test, once the fracture is initiated, the fracture propagation takes place instantaneously because the region close to the crack is under a state of uniaxial tensile stress; consequently, the failure load is slightly larger than the crack initiation load. In a borehole jack-loading, the areas around the "initiated cracks" are under a polyaxial state of stress. Consequently, the borehole jack tensile strength must be much larger than the flexural strength. It should be noted that Bianiawski has found experimentally that under a polyaxial state of stress, the failure load can be as large as three times the crack initiation load (Bianiawski, 1965).

The borehole tensile strengths determined from the failure of plaster-celite and concrete blocks, having central circular openings, by an increasingly applied uniaxial in situ stress field, support the argument above. The tensile strengths obtained from these tests are larger than the flexural strengths. For plaster-celite, the average borehole tensile strength was found to be 2.1 times the average flexural strength; the ratio was found to be 2.3 for concrete. It should be mentioned that this mode of loading is slightly different from the borehole jack loading. The tensile stress is maximum along two lines;

i.e., $\theta=0$ and π, instead of four lines, and there is no abrupt change from tensile to compressive stress at these locations.

For narrow bearing plates, the contact stress is approximately uniaxial and uniform; i.e., $k \approx 1$; therefore, from the failure load corresponding to a small plate angle β, the borehole tensile strength can be calculated from the following equation:

$$T_B = K_T(k,\beta) \frac{P_F}{R} \quad , \tag{2-1}$$

where: T_B = borehole tensile strength;

$K_T(k,\beta)$ = maximum tensile stress factor with k=1;

P_F = failure load;

R = radius of the borehole.

As stated early in this chapter, the ratio of the calculated borehole tensile strength, T_B, and the average flexural strength, T_S, is defined as the borehole strength ratio, L_r. This ratio was found to be 2.5 for plaster-celite, and 2.9 for concrete. The theoretical strength ratio, L_r, determined from borehole jack tests, is slightly larger than the actual strength ratio because of the reduction of the stress factor K_T. The actual maximum tensile stress factor is slightly smaller than the theoretical factor, $K_T(k,\beta)$, because of the yielding and the geometrical change discussed earlier.

The strength ratio, L_r, is essentially constant for a given material. In weak materials, the effect of yielding and geometrical change during loading is more significant; therefore their strength ratios, L_r, should be greater than those for elastic materials.

Determination of the Boundary Stress Factor, k

The boundary stress factor, k, describes the shape of the distribution curve of the contact stress between the bearing plates and the walls of the opening. It is a property of the jack and rock material which has to be determined experimentally. The problem of borehole jack loading is solved once the proper boundary stress factors are determined.

From the testing of a material with the experimental borehole jack using different sets of bearing plates, a curve of failure load as a function of the plate width (in terms of the angle β) can be drawn. On the same graph, the fracture initiation load curves (using the flexural strength T_s) corresponding to different values of k are drawn (Figures 2-4 through 2-7). For a given plate width angle, β, the appropriate factor k can be determined as follows:

1. Divide the failure load by the borehole strength ratio, L_r, to obtain the proper fracture initiation load.

2. With the calculated fracture initiation load, the appropriate value of k can be interpolated from the graph.

The strength ratio, L_r, and the factors k for the tested plaster-celite and concrete are given in Table 2-2. Once k is determined, the maximum stress factors, $K_{IT}(k,\beta)$ and $K_{IIT}(k,\beta)$, corresponding to Problems I and II, respectively, can be obtained from Tables 2-3 and 2-4. The numerical values of the stress factors as presented in Tables 2-3 and 2-4 were calculated as described by Van and Goodman (1970).

The strength ratio L_r and the boundary stress factors k for brittle elastic rocks should be approximately equal to those for plaster-celite material. For weak rocks, the parameters determined for weak concretes are more appropriate. More accurate values of k and L_r for different types of rock can be determined with a jack which can exert enough load to induce the fracturing of rock model plates. The average applied pressure for such a jack is in the order of the flexural strengths of the rock substances.

INTERPRETATION OF NX-BOREHOLE JACK TEST RESULTS

The available NX-borehole jack (Goodman Jack, Slope Indicator Inc., Seattle, Washington) can apply a maximum load of 20,000 lbs-per-inch of bearing plate length. Such a jack load is sufficient to induce tensile fracturing of an NX-size borehole under most field conditions. Some modification could be made to further increase the load. The device has been used to measure the deformability of concrete in the laboratory and the in situ deformability of rock and concrete masses at a number of engineering sites (Van, 1967; Goodman, Van, and Heuzé, 1968).

Table 2-2. Boundary stress distribution factors k for concrete and plaster-celite, determined experimentally.

Bearing Plate Angle β		5°	25°	45°	65°	85°
Concrete $L_r = 2.9$	Solution I	1.0	0.9	0.8	0.7	0.5
	Solution II	1.0	0.6	0.8	1.8	5.5
Plaster-celite $L_r = 2.5$	Solution I	1.0	0.7	0.5	0.4	0.4
	Solution II	1.0	0.5	0.6	1.2	4.5

Table 2-3. The stress factor $K_{IT}(k,\beta)$ as a function of the boundary stress distribution factor k and the bearing plate width angle β.

k	5°	15°	25°	35°	45°	55°	65°	75°	85°
0.1	-.85	-.91	-.95	-1.05	-1.10	-1.15	-1.20	-1.26	-1.39
0.3	-.96	-1.02	-1.08	-1.18	-1.32	-1.43	-1.53	-1.65	-1.85
0.6	-1.09	-1.16	-1.24	-1.37	-1.60	-1.78	-1.95	-2.14	-2.45
1.0	-1.22	-1.30	-1.40	-1.55	-1.88	-2.15	-2.39	-2.66	-3.11
2.0	-1.43	-1.51	-1.66	-1.85	-2.35	-2.75	-3.15	-3.60	-4.33
5.0	-1.68	-1.78	-1.98	-2.23	-2.95	-3.56	-4.18	-4.94	-6.21
10.0	-1.81	-1.92	-2.15	-2.44	-3.28	-4.02	-4.80	-5.77	-7.46

2-24

Table 2-4. The stress factor $K_{IIT}(k,\beta)$ as a function of the boundary stress distribution factor k and the bearing plate width angle β.

k	5°	15°	25°	35°	45°	55°	65°	75°	85°
0.1	-0.82	-0.93	-1.01	-1.02	-1.01	-0.98	-0.94	-0.90	-0.87
0.3	-0.89	-0.98	-1.19	-1.26	-1.26	-1.22	-1.16	-1.07	-0.99
0.6	-0.99	-1.03	-1.40	-1.54	-1.57	-1.52	-1.43	-1.29	-1.15
1.0	-1.08	-1.22	-1.61	-1.83	-1.88	-1.83	-1.70	-1.53	-1.33
2.0	-1.22	-1.41	-1.95	-2.29	-2.39	-2.35	-2.19	-1.95	-1.66
5.0	-1.40	-1.63	-2.38	-2.86	-3.04	-3.03	-2.85	-2.55	-2.16
10.0	-1.50	-1.76	-2.16	-3.17	-3.40	-3.41	-3.24	-2.93	-2.50

Borehole jack loads are applied and increased incrementally until failure occurs. The slopes of the load-deformation curves are used to calculate the modulus of deformability (Van, 1967). The failure loads are used to determine the borehole flexural strength (as differed from the flexural strength determined from flexural tests) which is equal to the borehole tensile strength T_B divided by the borehole strength ratio, L_r. Strengths of concretes were determined in the laboratory. A limited amount of borehole jack test results obtained for limestone masses at the Crestmore Mine, Riverside, California, were interpreted to obtain the tensile strength of the limestone.

Concrete blocks with a central 3-inch-diameter opening were cast for the study of the effect of the in situ stress field on the borehole jack test results. A uniaxial in situ stress field was simulated with a testing machine; borehole jack loading was then introduced and slowly increased in very small increments until failure. Tensile strength and the magnitude of the in situ stress field were computed from the borehole jack test results and compared to the known values. A device for the simulation of a biaxial in situ stress field was not built because of time and cost factors; furthermore, the uniaxial stress field is in effect a biaxial stress field with one principal component equal to zero.

Tensile Strength Determination by Borehole Jack Test

Flexural strength determined by borehole jack is obtained by dividing the borehole strength, T_B, by the strength ratio, L_r.

Tensile strengths of concretes.

For concretes, the borehole strength ratio $L_r = 2.9$ was used. From Table 2-2, the boundary stress factor k was found to be equal to 0.8 for a bearing plate width angle $\beta = 45°$. From Table 2-3 the maximum tensile stress factor, K_{IT}, was found by interpolation to be equal to 1.75.

Thick-walled cylinders made of a strong nonhomogeneous concrete with an inner diameter of 3 inches and outer diameter of either 18 inches or 24 inches were tested with the NX-borehole jack.* The in situ stress field

---

* Tests were made in 1967 by the author in the study of in situ measurement of rock deformability by borehole jack devices (Van, 1967).

was zero, and the cylinders were unrestrained from the outside. The flexural strength, T_S, was obtained by rupture tests of concrete beams. The borehole tensile strength, T_B, was calculated from the Equation (1-4), with $p_1 = 0$. The borehole flexural strength was obtained by dividing the calculated T_B by the strength ratio $L_r = 2.9$. The results are tabulated in Table 2-5.

Concrete blocks, 12 inches square and 5 inches in thickness with a 3-inch central circular opening, were cast for the study of the effect of a uniaxial in situ stress field on borehole jack test results. The content of the concrete mixture was 64% by weight of No. 20 "Lapis Lustre" fine sand, 23% of Portland cement Type I, and 13% of water. The concrete blocks were cured under a constant temperature of 68° and 100% relative humidity for nine days before testing. Concrete beams 6 inches × 6 inches × 24 inches were cast for the rupture tests.

To insure more uniform distribution of the applied uniaxial load from the testing machine, two wooden blocks were placed above and below the concrete block (Figure 2-14). The uniaxial load represents the in situ stress field; this load was applied first. The borehole jack was then placed into the central opening and turned into the desired orientation (the angle α is chosen). Jack loading was applied at 158-lb increments (10-psi intervals on pressure gage) up to failure. The jack orientation (angle α), the uniaxial in situ stress field p_1 and the failure jack load were recorded. Borehole tensile strength T_B was calculated from the Equation (1-6) with $p_2 = 0$. The borehole strengths and the flexural strength by rupture tests were tabulated in Table 2-6.

The failure loads used for the interpretation of strengths and stresses were the applied jack loads when very small cracks were observed. After the cracks were formed, additional applied loads caused the crack lengths to increase. The jack loads to cause the cracks to reach the edges of the concrete blocks were from 2.5 to 3.4 times the failure loads. For the cases of zero in situ stresses, once cracks were formed, they propagated instantaneously to the edges, splitting the concrete blocks.

Once cracks form, the overall geometry changes; therefore, the theory presented applies only to the conditions where the cracks are just formed.

Table 2-5. Borehole strengths of a nonhomogeneous concrete.

Test No.	Borehole tensile strength, T_B (psi)	Borehole flexural strength, T_B/L_r (psi)	Rupture flexural strength, T_S (psi)	Remarks
1	-2060	-710	average:	$L_r = 2.9$
2	-1980	-685	-588	in situ
3	-2290	-790		stress
4	-1915	-660	range:	field = 0
5	-2110	-727	from -518	
6	-2190	-754	to -646	

(b)

(a)

Fig. 2-14. A concrete block subjected to a uniaxial in situ stress, p_1, and to borehole jack loading.

2-29

Table 2-6. Borehole strength of a homogeneous concrete under uniaxial in situ stress.

Test No.	Jack orientation, α ($^\circ$)	Uniaxial in situ stress, p_1 (psi)	Borehole tensile strength, T_B (psi)	Borehole flexural strength, T_B/L_r (psi)	Rupture flexural strength, T_S (psi)
1	$\alpha = 90$	30	-1160	-398	
2	$\alpha = 90$	100	-1080	-373	
3	$\alpha = 0$	205	-1256	-433	average:
4	$\alpha = 45$	205	-1195	-412	-385
5	$\alpha = 45$	310	-1250	-430	range:
6	$\alpha = 45$	310	- 976	-336	from -356
7	$\alpha = 45$	400	-1300	-448	to -410
8	$\alpha = 0$	400	-1190	-410	

2-30

Consequently, the detection of small radial cracks is essential to the accurate determination of the failure loads. Inaccurate values of failure loads could lead to very poor and misleading stress interpretation. The effect is less in the strength investigation.

Tensile strength of Riverside Limestone.

Borehole jack testing was a part of an in situ investigation project done on the underground limestone masses at the Crestmore Mine, Riverside, California (Heuzé and Goodman, 1970). Tests were made with the NX-borehole jack (Goodman jack) in vertical and horizontal NX-boreholes at two mine levels. A number of tests were also made earlier by the authors in the study of the in situ determination of rock deformability by borehole devices (Van, 1967; Goodman, Van, and Heuzé, 1968). Two borehole jack orientations were used; the angle α was equal either to zero or $\pi/2$. The two orientations correspond to the same Equation (1-9). The two chosen orientations were not independent; therefore, the results could not be used to estimate the principal components of the in situ stress field.

Borehole jack loads were applied and increased incrementally up to 20,000 lbs/inch of bearing plate length. A large number of load-deformation curves were found to have a marked change in their slopes at the approximate jack load of 14,000 lbs/inch. This change in slope was caused by the presence of induced tensile cracks; tensile cracks were observed when the jack was placed in a vertical borehole such that the tops of the bearing plates were at the floor of the test gallery.

The magnitude of the principal stress components of the in situ stress field was determined by overcoring. It is not possible to pinpoint the failure loads from the load-deformation curves; the presence of small cracks does not cause a visible effect on the straight line deformation behavior of the borehole. However, when the crack lengths become large, the reduction in the slopes of the load-deformation curves are visible; and these crack lengths can be estimated (Goodman, Van, and Heuzé, 1968).

In the calculation of strengths, the jack load corresponding to the marked change in the slope of the load-deformation curve was arbitrarily taken as the failure load. The radius of the borehole was replaced by the estimated distance from the center of the opening to the tip of the crack. The effect of this arbitrary procedure on the results is not known.

Limestone is practically linearly elastic; therefore, the borehole strength ratio L_r and the boundary stress factor k for plaster-celite can be reasonably used. From Table 2-2 we have L_r = 2.5 and k = 0.5. From Table 2-3, K_{IT} was found by interpolation to be 1.51. The borehole tensile strength T_B, the borehole flexural strength T_B / L_r, and the flexural strengths determined from rupture tests are given in Table 2-7.

The average flexural strengths determined by borehole jack tests were slightly larger than the average flexural strengths determined by rupture tests. The difference was 9% for the homogeneous concrete, 23% for the nonhomogeneous concrete, and 32% for the Riverside Limestone.

The large difference between the borehole flexural strength and the flexural strength by rupture test of limestone could be partially caused by the inaccurate determination of the principal components of the in situ stress field. Most of the tests were made at shallow depths; i.e., very close to the free face. In these regions the stress components change very rapidly with depth (the values p_1 and p_2 used for the calculation of the borehole strengths were the stress components at the middle of the bearing plates). Part of the errors is attributed to the arbitrary calculation procedure in which a special jack load and the radial distance to the crack tip were used in the places of the failure load and the radius of the opening.

Stress Determination by Borehole Jack

Once the borehole tensile strength of a rock mass and the principal direction of a biaxial in situ stress field are known, the principal stress components can be determined by borehole jack test results. Two properly chosen jack orientations at the same point in the same borehole provide two independent equations in which the components p_1 and p_2 are the unknowns. It should be remembered that the borehole tensile strength is "equal" to the flexural strength multiplied by the strength ratio L_r. For a borehole jack with an angle β = 45° the angle made between two chosen orientations must be different than $\pi/2$ to provide two independent equations.

The magnitude of a uniaxial in situ stress field is determined from a borehole jack test by the following equation:

$$T_B = p_1 \{1 - 2\cos 2(\beta - \alpha)\} + K_T(k,\beta)\frac{P_F}{R} . \qquad (2-2)$$

Table 2-7. Borehole strengths of Riverside Limestone.

Test no.	In situ stress field (overcoring)		Borehole tensile strength	Flexural strength by borehole jack test, T_B/L_r	Flexural strength by rupture test, T_S
	p_1	p_2			
1	1800	600	-4500	-1800	
2	1900	900	-4380	-1750	
3	700	300	-6060	-2420	
4	600	300	-6480	-2600	average:
5	600	300	-7700	-3100	-1780,
6	700	300	-6760	-2700	range:
7	1100	400	-4760	-1900	from -1560
8	1100	300	-6340	-2540	to -2080
9	700	400	-6070	-2430	
10	900	400	-6300	-2520	

The calculated values of p_1 are compared to the applied stresses p_1 in the testing of concrete blocks (Table 2-8). In all the calculations for p_1 which were reported in Table 2-8, the stress p_2 was assumed to be known and equal to zero. Even if both stress components were unknown, the results of tests No. 3 and No. 4 provided two equations from which we could solve for p_1 and p_2. The calculated p_1 was equal to 285 psi as compared to the applied p_1 of 205 psi; the calculated p_2 was equal to 45 as compared to the applied p_2 of zero. For tests No. 7 and No. 8, the calculated p_1 was 439 as compared to the applied value of 400; the calculated p_2 was 36 psi as compared to the applied p_2 of zero.

From the testing of concrete blocks under a uniaxial in situ stress field, the calculated stress components checked fairly well with the actual applied stresses for large stress components. The difference between the applied in situ stress components and the computed values from the borehole jack test results was very large for low stress fields. This difference can be partially attributed to the inaccurate measurement of the flexural strengths. Any error in the flexural strength T_S is multiplied by the strength ratio L_r in the calculation of in situ stress components.

In stress calculation, any error in the failure load is also multiplied by the strength ratio L_r. Therefore, for the in situ measurement of stresses, the borehole jack must be equipped with a crack detecting device so that the failure load can be determined accurately. The crack detecting device is essential because the errors associated with the failure loads could be much larger than the measured stresses, especially when the in situ stress components are small as compared to the tensile strength of the rock substance.

CONCLUSIONS

From the experimental studies with the experimental jack and the NX-borehole jack, a number of conclusions can be made:

1. Under borehole jack loading, a circular opening in a brittle solid fails by tensile fracturing when the bearing plate width is not too small. The tensile cracks are normally formed at the edges of the bearing plates; these locations are in agreement with the theoretical prediction.

Table 2-8. Comparison of the applied uniaxial stress p_1 and the calculated p_1.

Test no.	Jack orientation	Applied p_1 (psi)	Calculated p_1 (psi)	Remarks
1	$\alpha = 90°$	30	70	
2	$\alpha = 90°$	100	60	
3	$\alpha = 0°$	205	286	$L_r = 2.9$
4	$\alpha = 45°$	205	135	$k = 0.8$
5	$\alpha = 45°$	310	388	$K_{IT} = 1.75$
6	$\alpha = 45°$	310	356	
7	$\alpha = 45°$	400	448	
8	$\alpha = 0°$	400	410	

2. In some tests, cracks are formed at the locations $\theta = \pi/2$ and/or $\theta = -\pi/2$: the occurrence of these cracks can be explained by considering the actual behavior of the material around the opening during the loading.

3. The two proposed contact stress distributions can reasonably explain the mechanism of tensile fracturing by borehole jack loading: either solution can be used, providing the appropriate stress factor k is used;

4. The contact stress distribution factor k is a material property which can be determined experimentally;

5. The borehole tensile strength, T_B (the failure stress under the polyaxial borehole jack loading), is larger than the rupture flexural strength, T_S, as expected. The strength ratio $L_r = T_B/T_S$ is relatively a constant; the strength ratio is also a material property and can be determined experimentally.

6. Knowing the magnitude and orientation of the in situ stress field, borehole jack test results can be used to determine the borehole tensile strength, T_B. The flexural strength of the rock substance can be calculated, using the appropriate strength ratio L_r.

7. Knowing the orientation of the in situ stress field and the flexural strength of the rock substance, the magnitude of the in situ stress components can be calculated. Two properly chosen jack orientations lead to two independent equations which are used to solve the stress components.

8. The detection of very small tensile cracks is essential for the accurate determination of the failure loads which are used in the calculation of strengths and stress components. There is, therefore, a definite need to develop a crack detection technique. Such a technique may be based on a device measuring rock noise, or increase in permeability or resistivity, for example. A borehole jack to be used in the field for the investigation of stresses and strengths in rock should be equipped with such a device.

REFERENCES

Absi, E. and Seguin, M., "Le Nouveau Geoextensometre," Supplement to
Annales de L'Institut Technique du Batiment et des Travaux Publics.,
No. 235-236, pp. 1151-1158, July-August 1967.

Bieniawski, Z. T., "Mechanism of Brittle Fracture of Rock," CSIR Report
MEG 580 (Pretoria, South Africa), 1967.

Chercasov, I. I., "The Residual Deformations Caused by the Deep Penetration
of a Rigid Plate into a Brittle Porous Material," in *Proc. Geotech.
Conf.* (Oslo 1967), vol. 1., pp. 179-180.

Goodman, R. E., Van, T. K., and Heuzé, F., "The Measurement of Rock
Deformability in Boreholes," *Proc. 10th Symposium on Rock Mechanics,
AIME* (1968).

Heuzé, F. E., and Goodman, R. E., "The Design of Room and Pillar Structures
in Competent Jointed Rock," *Proc. 2nd Congress of the Intern. Soc. for
Rock Mechanics,* Belgrade, 1970, Vol. 7, No. 4-41.

Obert, L., and Duvall, W. I., *Rock Mechanics and the Design Structures
in Rock*, John Wiley, New York, 1967.

Van, Tran K., "In-situ Determination of Rock Deformability by Borehole
Jack Tests," unpublished M. S. Thesis, University of California,
Berkeley, California (1967).

Van, T. K., and Goodman, R. E., Chapter 1, Vol. III, Final Report
NASA Contract NAS 8-21432, Jan. 1970, Space Sciences Laboratory
Series 11 Issue 12.

Wyanecki, J., "Les Geoextensometres du Centre Experimental de Recherches
et d'Etudes du Batiment et des travaux Publics, Etude Experimentale
sur Modeles Reduits," *Laboratoire du Batiment et Travaux Publics,*
Supplement aux Annales, No. 246 (June 1968).

Chapter 3. A BOREHOLE JACK FOR DEFORMABILITY, STRENGTH, AND STRESS
MEASUREMENTS IN A 2-INCH BOREHOLE

R. E. Goodman, H. J. Hovland, and S. Chirapuntu

INTRODUCTION

Among the properties that should be established in the design of
rock or soil for structures are the quantities describing the *deformability*
and the load limit or *strength*. For most applications, it is not sufficient
to typify only the surficial soils; values must be ascribed to deformability
and strength for all segments of the soil profile to a depth of many feet.
In the case of underground or buried structures, the properties of the
surface soils may not even be of interest.

A borehole measurement is an appropriate way of gaining this infor-
mation. The preceding chapters discussed aspects of borehole measurement
technique. This chapter describes a tool especially devised for lunar
exploration and presents results of its use in simulated lunar soils.

EQUIPMENT AND MATERIALS
Equipment
Lunar borehole jack.

The borehole jack described in Chapter 2 of this volume was intended
for model studies in the laboratory and is not appropriate for actual lunar
use as it lacks the proper range and dimensions. The principles on which
it works, however, are identical to those of the lunar jack to be described.
A hydraulic cylinder mounted between two stiff plates acts to spread the
plates apart against the borehole walls when pressured (see Fig. 2-1,
Chapter 1). The spreading is measured by a displacement transducer and
the load is measured hydraulically.

Lunar requirements and previous work in the laboratory and in the
field established the following guidelines for design.

diameter of borehole	- 2 inches
displacement measuring accuracy	- 0.0001 inch or better
loading limit	- 3000 psi maximum plate pressure
length of loading plates	- five to six times diameter of borehole

maximum stroke of piston   - 3/4 inch

number of displacement transducers - one at each end.

The lunar borehole jack was designed accordingly. The testing plates were made five to six times longer than the borehole diameter to make the loading approach plane strain conditions. Figure 3-1 shows the assembled jack; the curved surfaces are the plates spread out laterally at the time the jack is loaded. Drawings and specifications for the jack are presented in the Appendix.

The main improvement over previous instruments is the increased stroke, which allows large deformations of the borehole. To accomplish this, the displacement transducers (Linear Variable Differential Transducers, LVDT's) were placed parallel to the borehole and the transverse motion to be measured was translated to longitudinal motion through a small wheel rolling on a 45° incline. This incline is shown in the Appendix (section EE of assembly drawing), and in Figure 3-2, which exhibits details of the disassembled borehole jack. By providing LVDT's at both ends, a nonparallel motion of the plates can be determined and corrected.

Twenty-eight pistons are used, as shown in Figure 3-2, to obtain a high hydraulic efficiency (ratio of piston to plate area). Three return pistons are also provided.

No attempt was made at this time to make the instrument small and light enough for transportation to the moon. It is a closed hydraulic system, however, and can be adapted to the lunar environment. The steel bench model weighs 4.6 kilograms; this can be greatly reduced by using aluminum or by making certain modifications in the design.

Based on experience gained during testing of the lunar borehole jack, the following minor modifications are suggested.

1. Addition of a bleed valve so that all air can be drained out of the hydraulic system.

2. Consideration of a more permanent membrane to prevent dust and soil particles from getting into the jack.
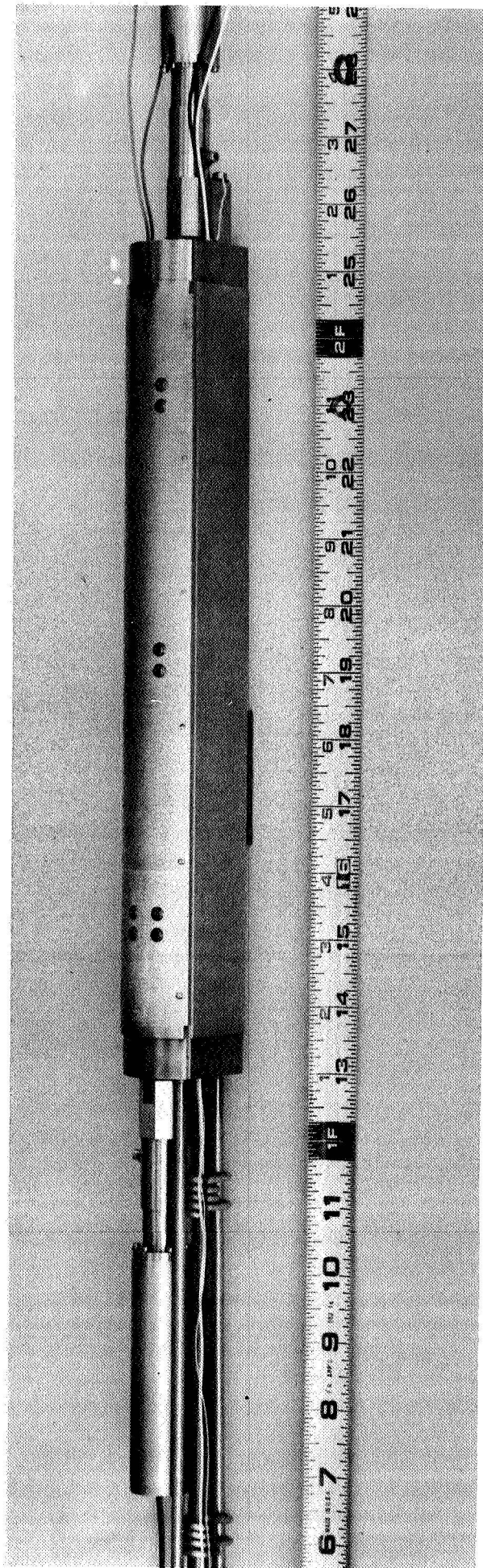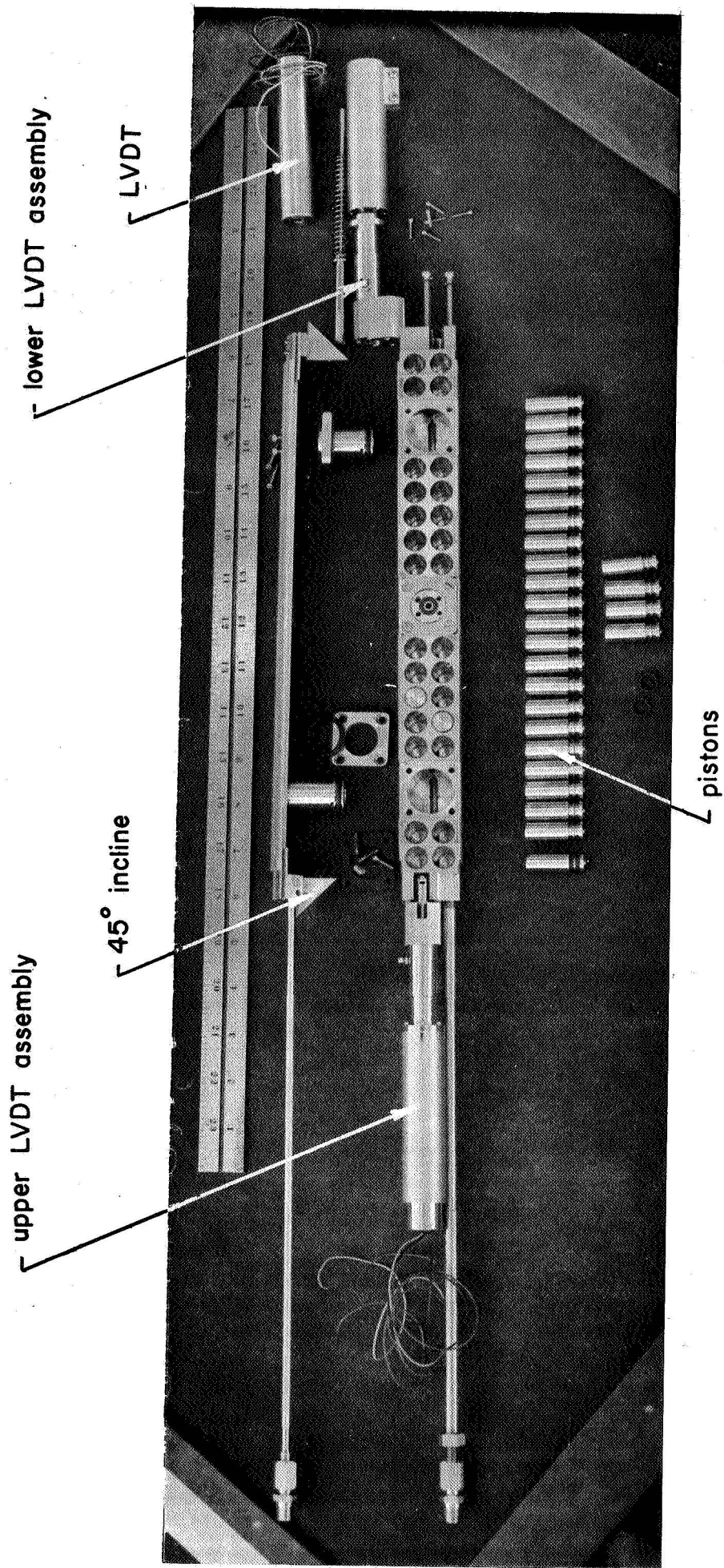
Fig. 3-1. Assembled lunar borehole jack.

Fig. 3-2. Disassembled lunar borehole jack.

3. Addition of optional resistive springs to be used in connection
with testing of loose soils to prevent the two ends of the jack
from moving nonuniformly.

4. Addition of a permanent steel cap to the lower end to protect
the LVDT. A similar cap or casing could be added to protect
the upper LVDT.

Testing apparatus.

The testing apparatus, including a steel chamber, electrical instru-
ments, and the borehole jack, are shown in Figure 3-3. Tests were
conducted (in earth environment) inside the cylindrical steel chamber
filled with simulated lunar soil. The chamber was pressured longitudinally
by three pistons acting on a steel end plate to simulate depth of burial
under plane strain conditions. The specifications of the chamber are:

depth   - 30 inches
inside diameter   - 23.5 inches
wall thickness   - 0.275 inch
maximum longitudinal vertical pressure, σ_v - 58 psi.

A cardboard tube was placed in the center of this chamber and soil
simulant added around it to form a 2-inch-diameter borehole. The tube
was later withdrawn through a hole in the end plate.

The pressure σ_v on the ends of the chamber was supplied by a hand
pump and measured with a Bourdon gage. The hydraulic pressure inside the
jack was recorded on an x-yy' recorder receiving the output of a pressure
transducer and was simultaneously displayed on a 1000-psi Bourdon gage
with least reading of 2 psi. The pressure measurement in the x-yy' plot
was readable to within 2 psi. Displacement measurements from the LVDT's
were automatically plotted against load during the test by the x-yy'
recorder. The precision of the LVDT's is better than 0.0001 inch, but
for the experiment with simulated soil, only a hundredth of an inch
accuracy was utilized.

Materials

The soil material used as the test specimen was Lunar Soil Simulant
No. 2 (LSS No. 2), a light gray silty basalt powder. The gradation and
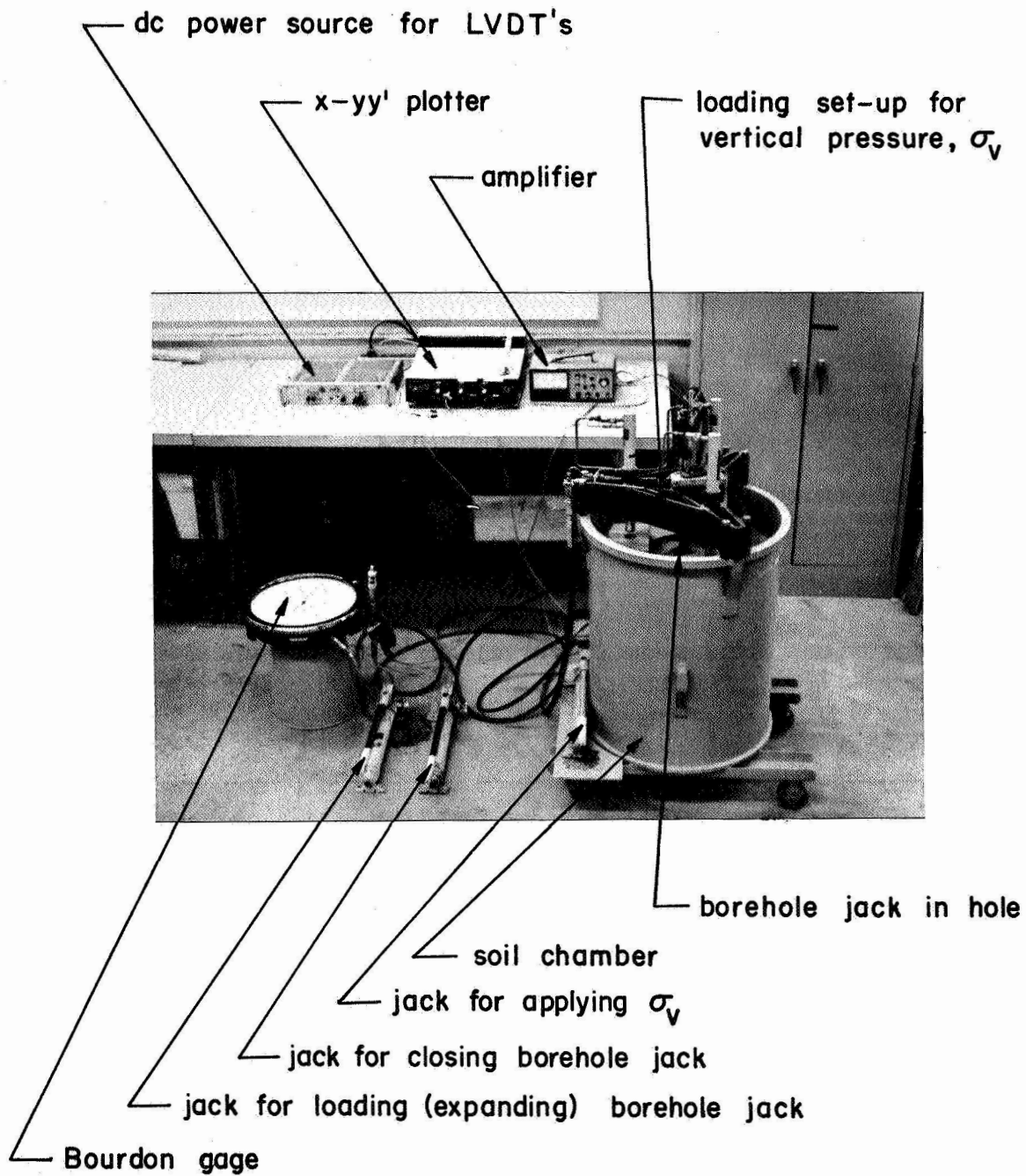properties of LSS No. 2 are reported in detail by Houston, Namiq, Mitchell,

Fig. 3-3. Assembly of borehole jack test set up.

and Treadwell, 1970. The moisture content and density of the soil were determined frequently during testing. The average values and ranges are listed in Table 3-1; since the cohesion is a known function of the water content, its value can also be listed.

TABLE 3-1

	Average	Range
Dry density	102 pcf (1.64 gm/cc)	94-109 pcf (1.51-1.75 gm/cc)
Moisture content	2.04%	1.9-2.17%
Cohesion	14.3 psf (7 gm/cm^2)	6.3-22.7 psf (3.1-11.1 gm/cm^2)

Since the LSS No. 2 at a moisture content of about 2.0 percent is believed to exhibit strength characteristics similar to actual lunar soil, all tests were run close to this moisture content, as shown above.

SPECIMEN PREPARATION AND TESTING PROCEDURE

Preparation of Specimens

To obtain a sample at a void ratio of 0.85-0.95, a method of sprinkling the soil from a given height of drop was used. A height of drop of 6 inches was used for obtaining a void ratio of 0.95, and 18 inches for a void ratio of 0.85. However, for a dense specimen of void ratio 0.75, the soil was also vibrated or tamped in 3-inch layers. A total of 650 pounds of soil was used for each test.

Testing Procedure

Lunar Soil Simulant No. 2 was placed in the chamber and the tests were conducted by the procedure outlined below.

1. Soil was placed to the height of 1 to 2 inches from the bottom of the chamber.
2. A cardboard tube of a diameter slightly larger than the borehole jack was placed in the center to cast the borehole.
3. Soil was deposited in the chamber by dropping it from a predetermined height and/or compacting and vibrating it in 3-inch layers to the desired density. After the chamber was filled, the circular metal end plate was placed on the top of the soil and the vertical pressure pistons were seated.

4. A no-load curve was obtained to calibrate the internal stiffness of the borehole jack without any external soil reaction. The rubber protecting sleeve (membrane) and piston O-ring friction are the source of the no-load resistance.

5. The cardboard tube was carefully pulled out and the borehole jack was inserted.

6. The test was done by expanding the borehole jack using a hand pump. The hydraulic pressure in the jack and deformation were recorded directly by an x-yy' plotter.

7. After the loading plates had been expanded through an appropriate range, the pressure was released and the expanded jack was closed by the return piston circuit using another hand pump.

8. The depth of soil in the chamber was measured to enable determination of the void ratio.

9. The borehole jack was turned 90° in the borehole and a higher vertical pressure was applied. Steps 6, 7, and 8 were then repeated. This repeated test was considered secondary in quality, and on the curves presented subsequently, the first (primary) tests conducted in undisturbed soil are represented by solid lines; the secondary tests are represented by dashed lines.

10. Moisture and density determinations were made for samples from the top, middle, and bottom of the chamber.

11. Tests at other vertical pressures and void ratios were run by repeating the above procedure (steps 1 through 10).

RESULTS

Pressure-deformation curves were obtained for each test using an x-yy' plotter. An example of such a curve is shown in Figure 3-4, where hydraulic jack pressure is plotted against increase of the borehole diameter. The lower portion of this figure shows a curve obtained with the jack out of the borehole; it gives the resistance caused by the rubber membrane and piston friction only. The upper curves show both soil resistance and resistance associated with the equipment.

It was also noted that the pressure-deformation curves were dependent on the rate of loading (rate of pumping the jack). Therefore, loading was intermittently discontinued for about 2 minutes, after which
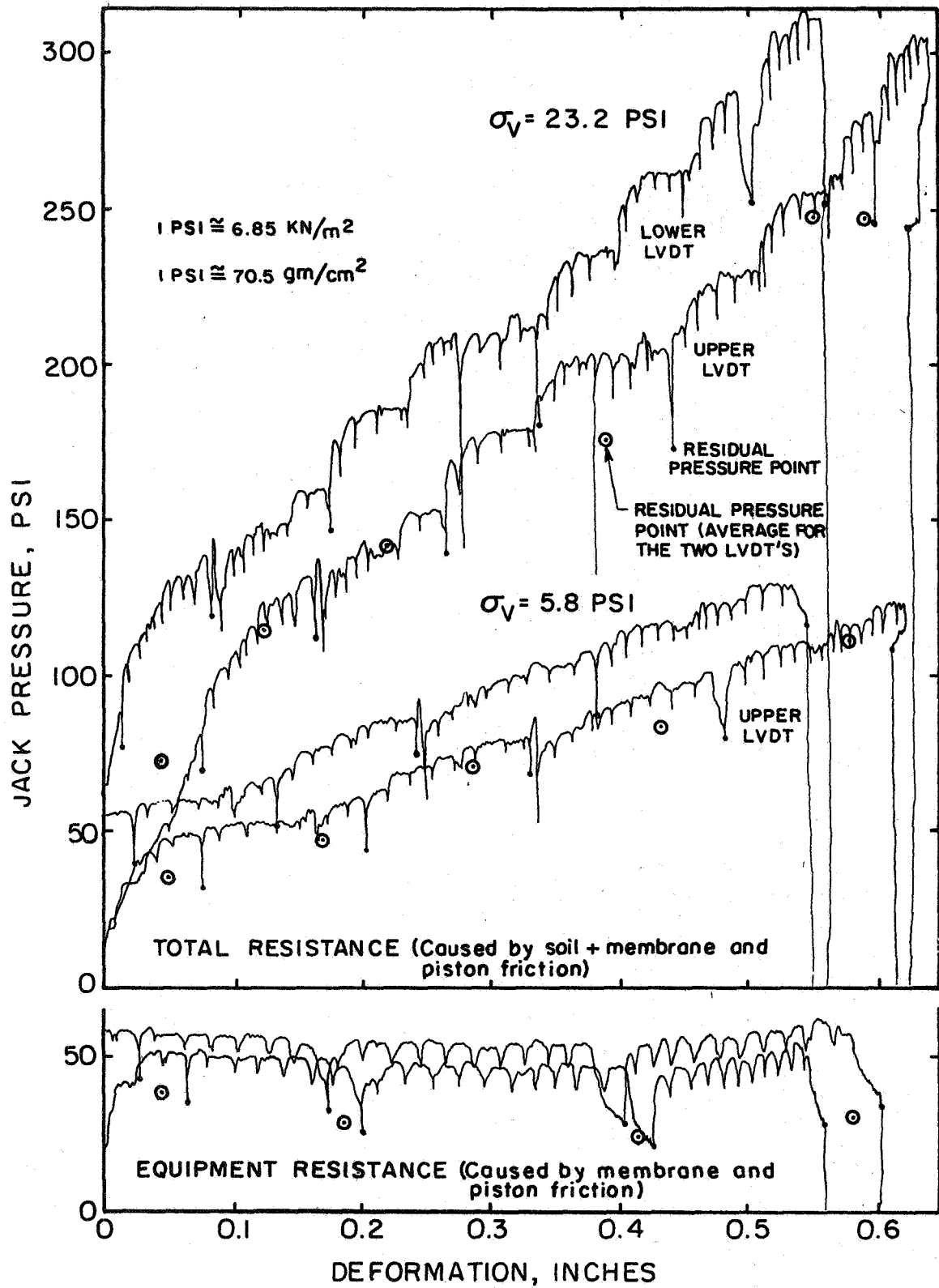
Fig. 3-4. X-YY' plot of pressure vs. deformation.

time pressure appeared to have dropped to a residual value. These pressures are also shown in Figure 3-4. Pore air pressure build-up and decline may explain part of this transient behavior.

Useful results were obtained from the x-yy' plotter curves, such as Figure 3-4, by considering the average residual pressure points only and deducting the resistance associated with the equipment from the total resistance. These curves were replotted and are shown in Figures 3-5 through 3-10. Two sets of points appear on these figures--open and closed symbols. The open symbols represent values obtained by deducting the average of all no-load curves from the total load curve. The closed symbols represent values obtained by deducting the preceding no-load curve from the total load curve. The curves in Figures 3-5 through 3-10 were drawn to give approximately equal weight to both sets of points.

DISCUSSION

According to Equation (1-10), the deformability of the borehole wall material can be expressed by

$$E = K \frac{\Delta P}{\Delta d / d} \ .$$

Using Equation (1-10), a modulus was determined for each curve in Figures 3-5 through 3-10 by finding a secant ratio of $\Delta P / \Delta d$ from the 0 to 0.25-inch deformation portion. The ratio of the pressure at the plate-soil contact to the hydraulic jack pressure is 0.263. Therefore,

$$\left. \frac{\Delta P}{\Delta d} \right)_{\text{for Eq. (1-10)}} = 0.263 \left. \frac{\Delta P}{\Delta d} \right)_{\text{Figs. 3-5 through 3-10.}}$$

The moduli determined as described above are plotted in Figure 3-11 as a function of the void ratio at the end of the test.

It is interesting to compare the moduli determined from the borehole jack tests with those determined from data on plate load tests shown in Figures 1-46, -47, -50, -51, and -52 of Vol. I, Chapter 1. The moduli from the plate load test data were computed using the appropriate

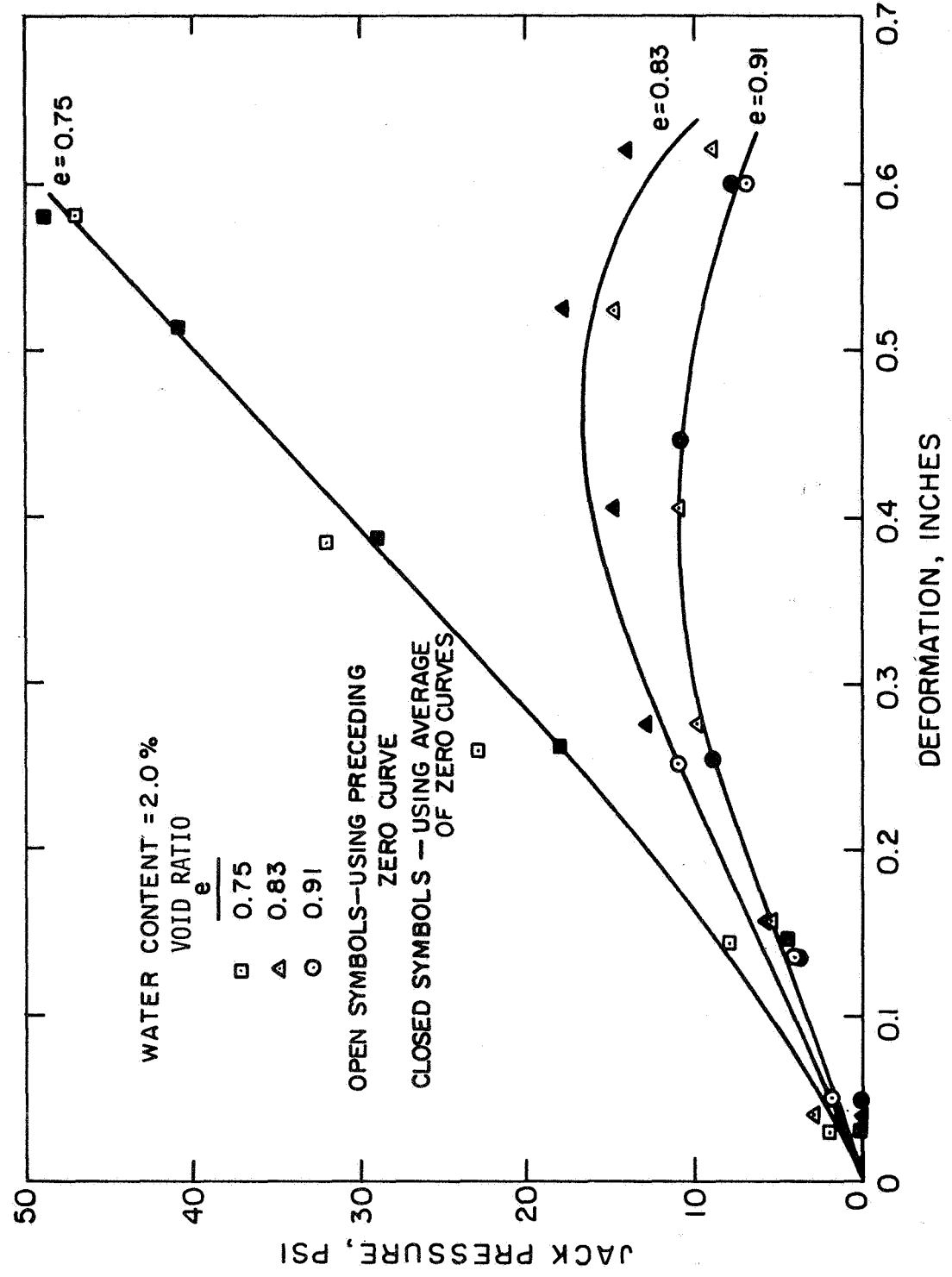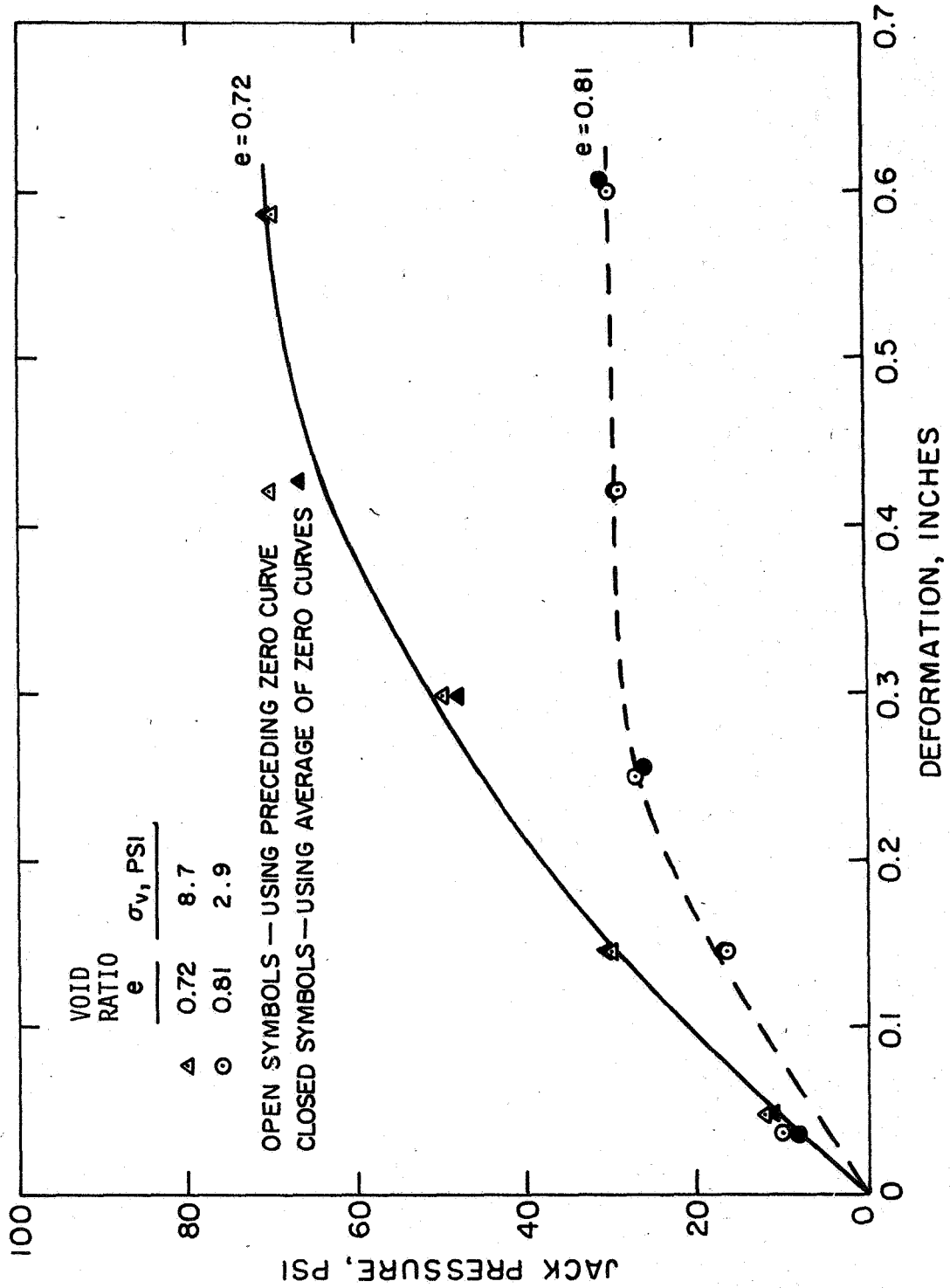Fig. 3-5. Pressure vs. Deformation, σ_v = 0.13 psi.

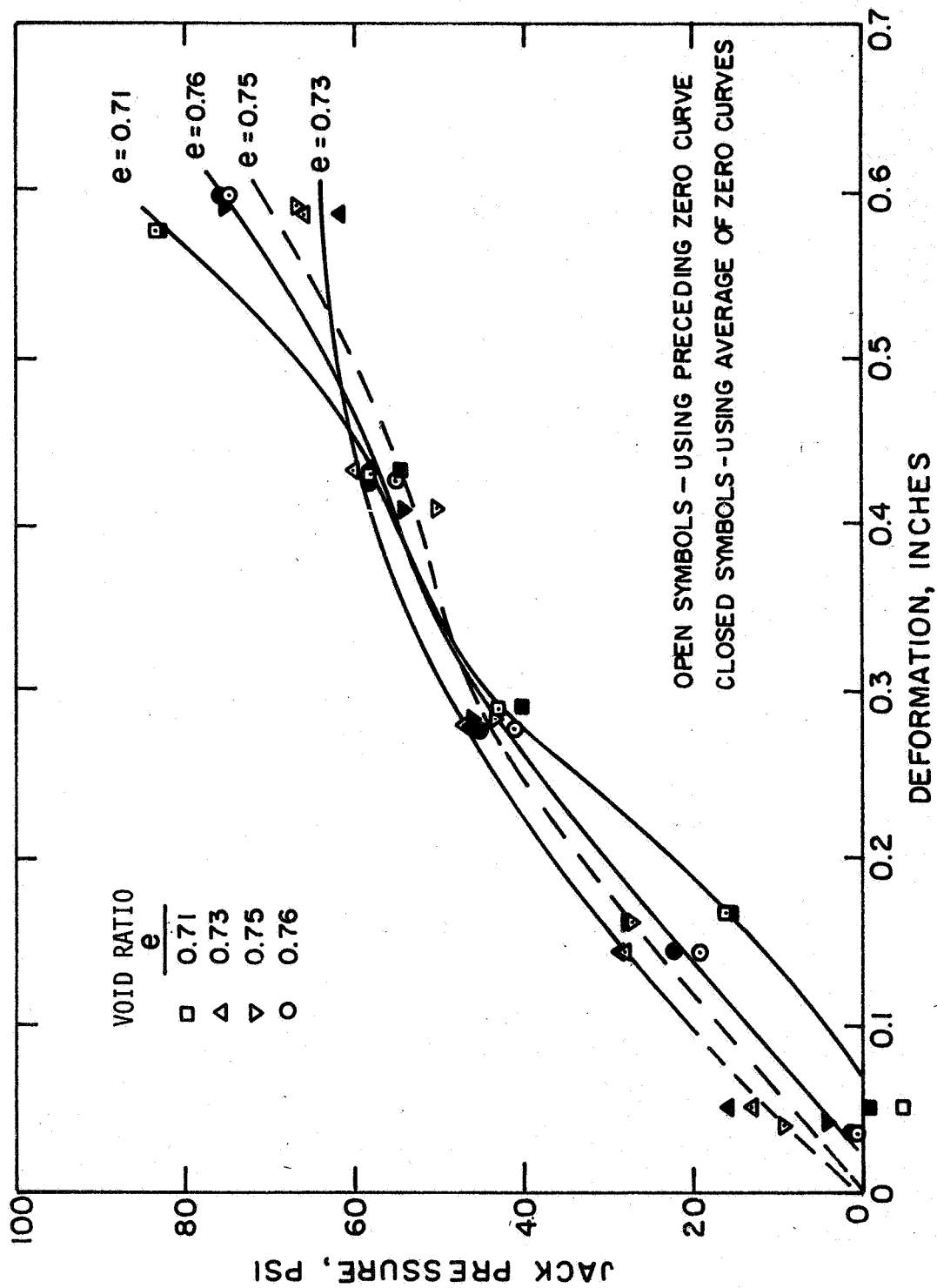Fig. 3-6. Pressure vs. Deformation, σ_v = 2.9 and 8.7 psi.

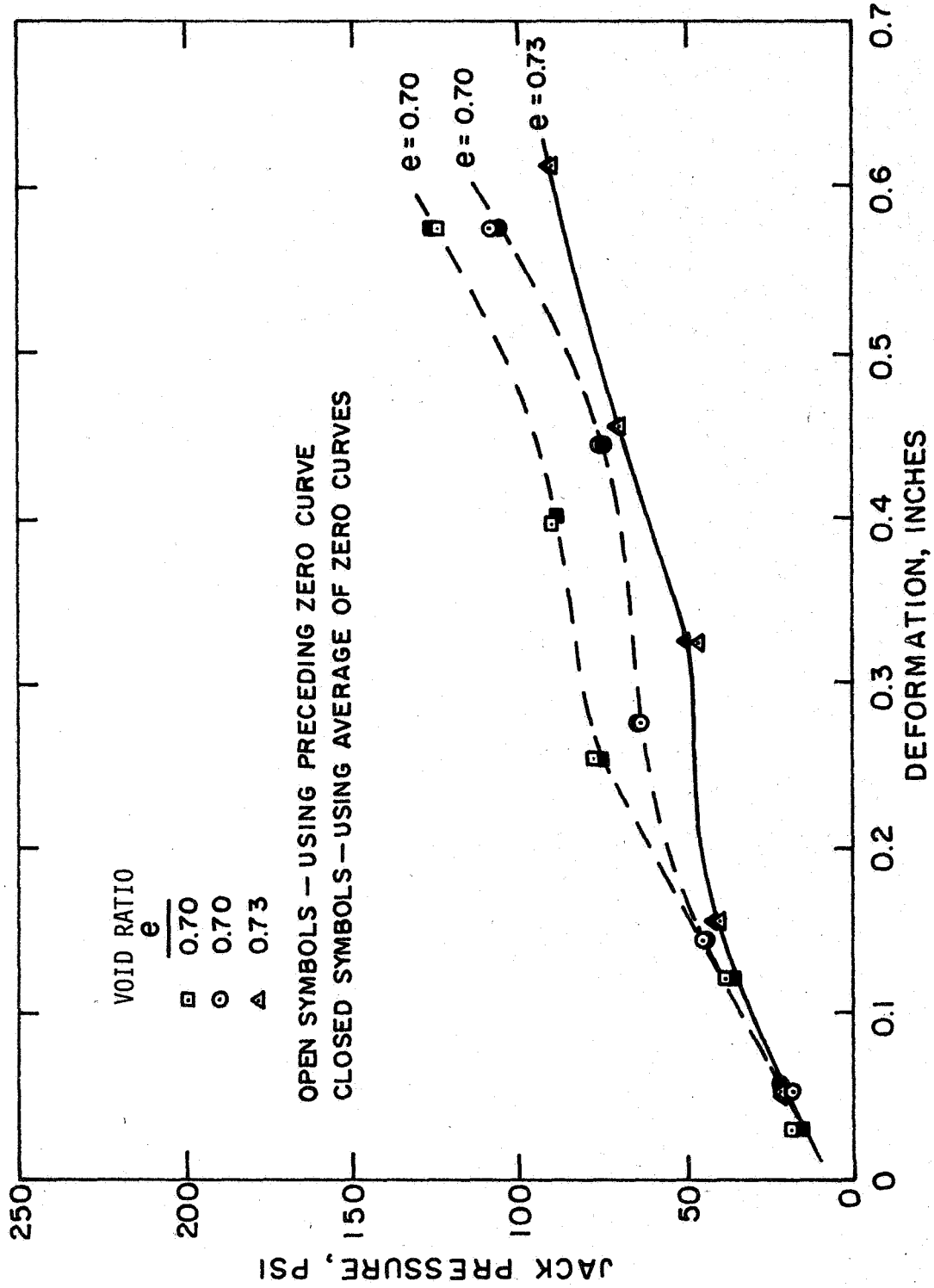Fig. 3-7. Pressure vs. Deformation, σ_v = 5.8 psi.

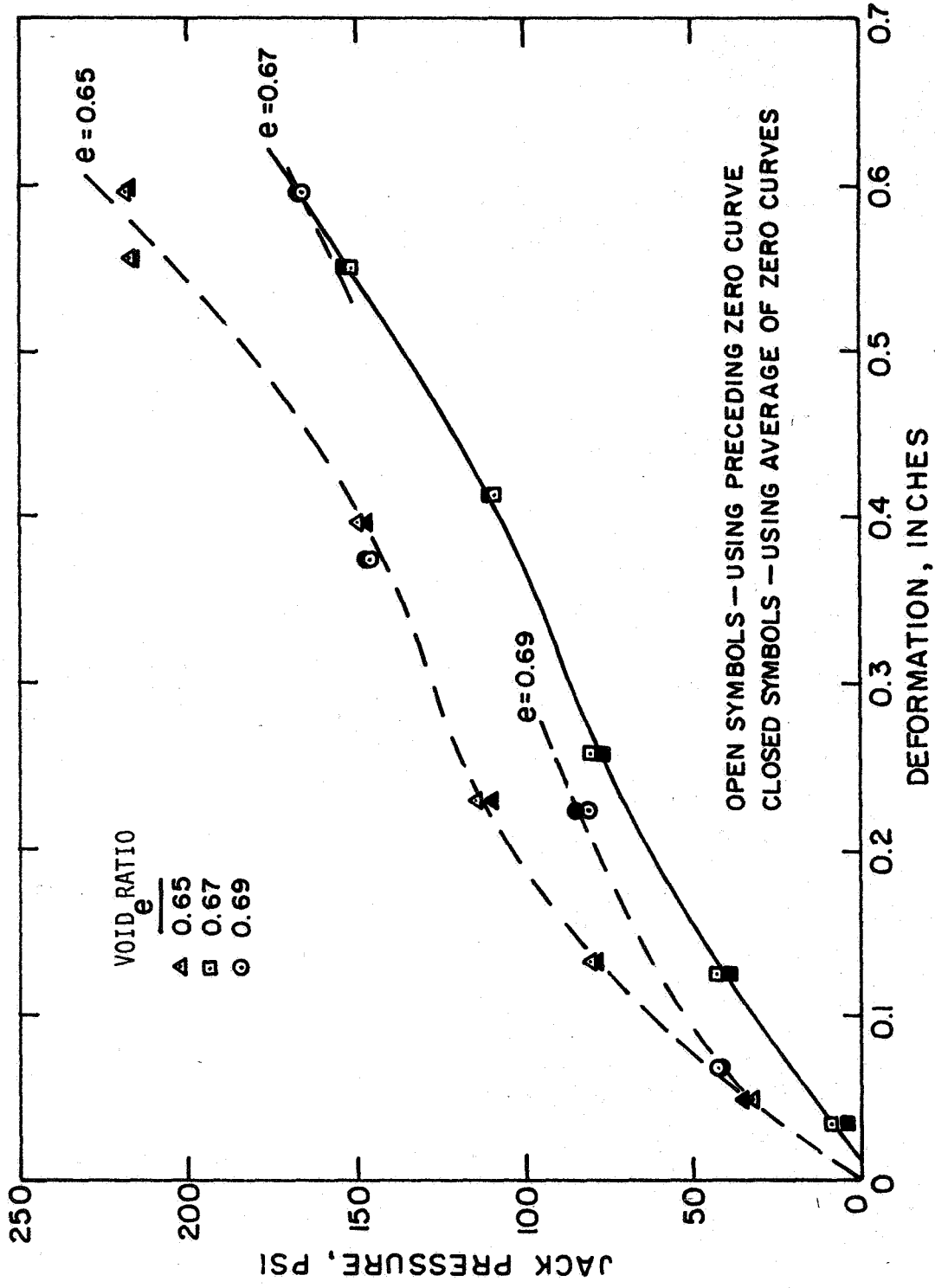Fig. 3-8. Pressure vs. Deformation, σ_v = 11.6 psi.

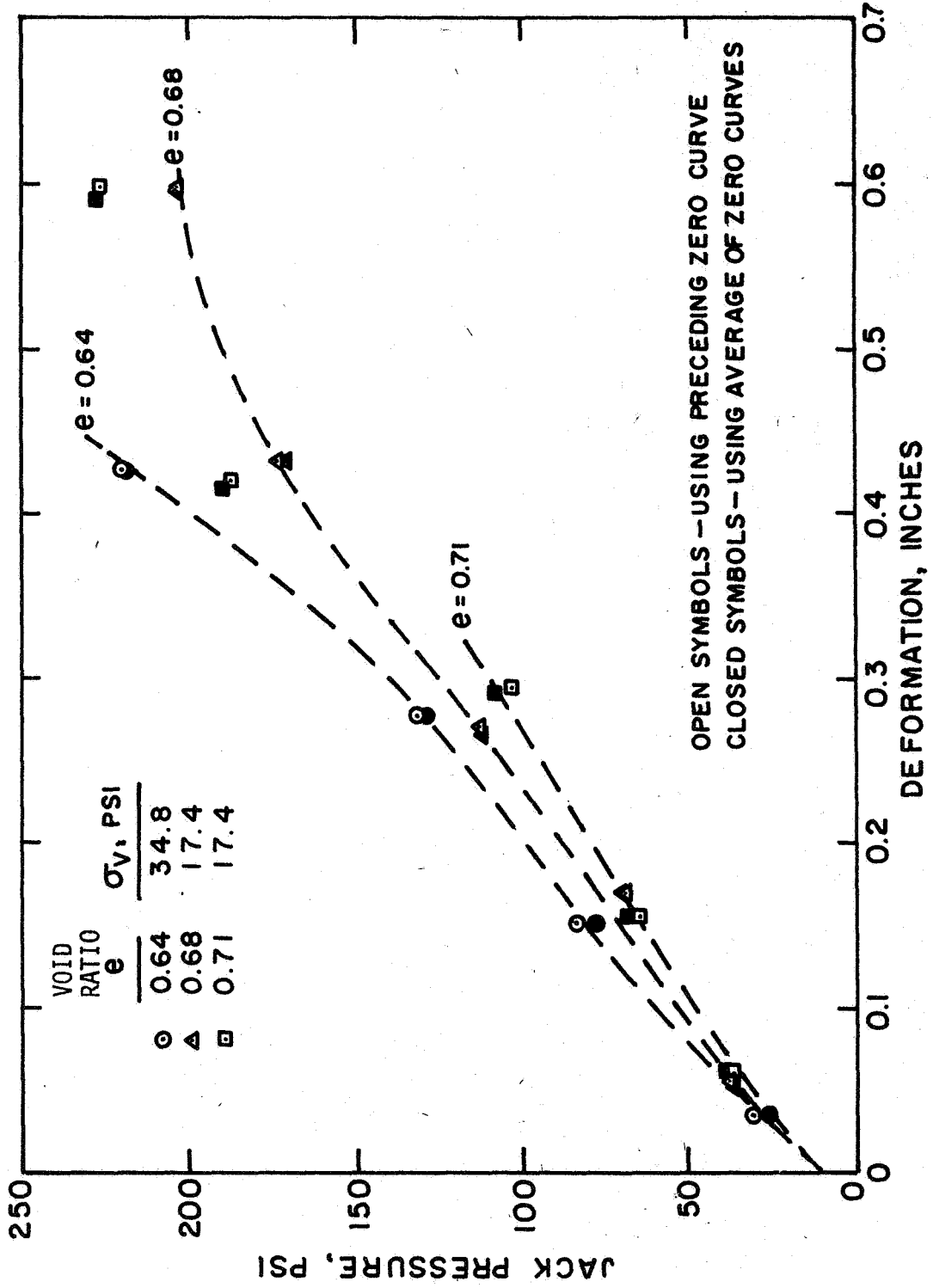Fig. 3-9. Pressure vs. Deformation, σ_v = 23.2 psi.

Fig. 3-10. Pressure vs. Deformation, σ_v = 17.4 and 34.8 psi.
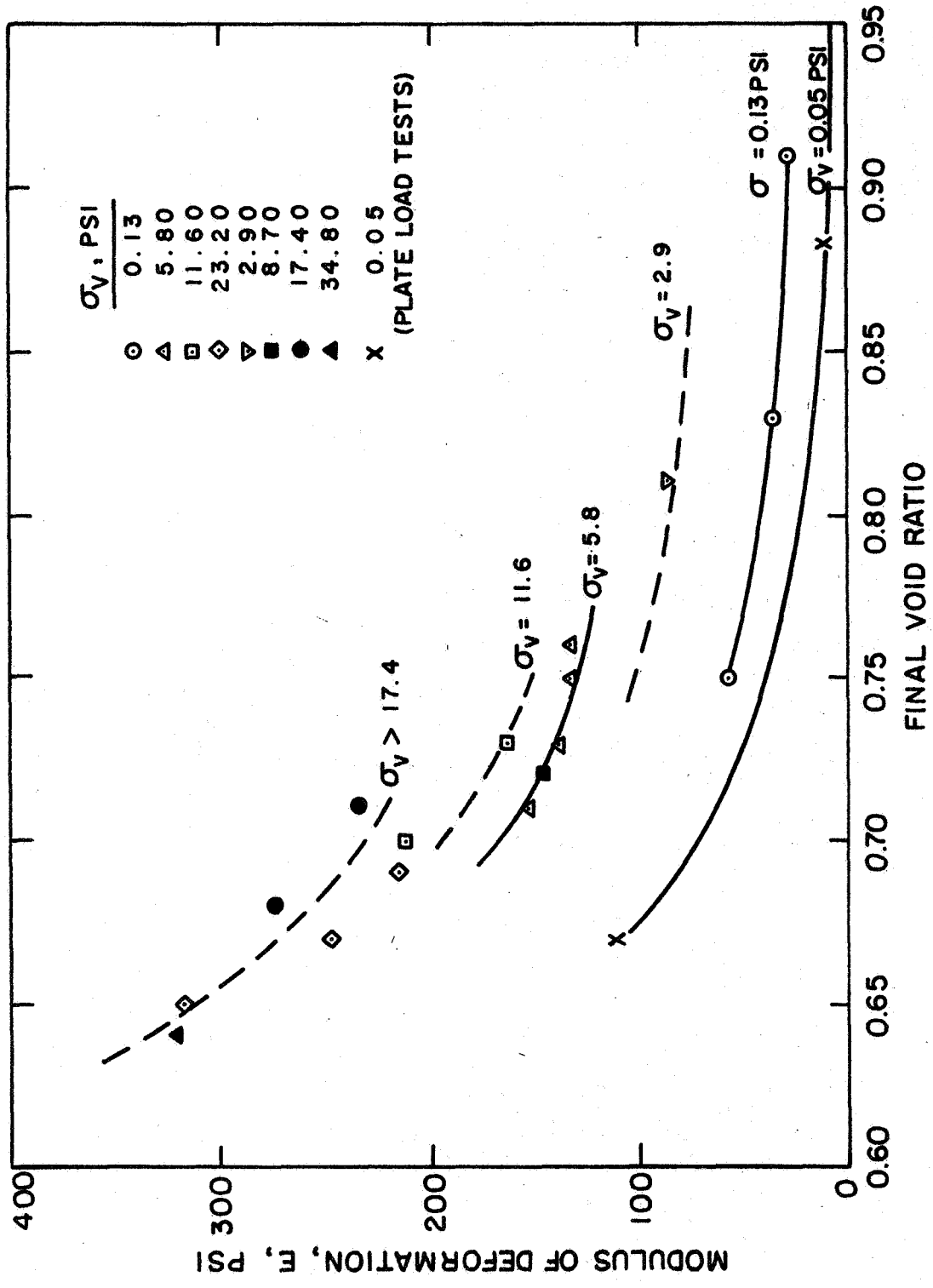
Fig. 3-11. Deformation modulus vs. void ratio.

equation from theory of elasticity (Terzaghi, 1943):

$$E = \frac{qB(1 - \mu^2)I_\delta}{\delta} \quad ,$$

(3-1)

where

$\quad$ q = uniform pressure

$\quad$ B = width of rectangular plate

$\quad$ μ = Poisson's ratio $\cong 0.35$

$\quad$ δ = vertical deformation, and

$\quad$ I_δ = influence factor.

The ratio of length to width of the plate was 5. For this ratio, the value of I_δ for a rigid plate on the surface of an elastic half-space is 1.6 (University of California, 1965). While I_δ = 1.6 is for a depth of infinity, the chamber in which the plate load tests were performed was about 80 cm deep, giving a chamber depth to plate width ratio on the order of 20. However, the modulus of deformability for the LSS No. 2 increases with depth; therefore, theoretically calculated deformations on the basis of a depth to plate width ratio of 20 would be too large. On the basis of such reasoning, a depth-to-plate width ratio of 5 was selected. Egorov (1958) investigated the influence of the depth to the rigid base. His values, reported by Harr (1966), indicate that the deformation for a depth of chamber to width of plate ratio of 5 is 0.808 times the deformation for a depth equal to infinity. Therefore, a value of I_δ = 1.6(0.808) = 1.29 was used. The moduli from the plate load test data, computed as described above, are presented in Table 3-2.

TABLE 3-2. Deformation moduli from plate load tests.

Test series	1	2	3
e_{ave} (depth 0-15 cm)	0.88	1.24	0.67
$E_{1'' \text{ plate}}$ psi	6	2.1	100
$E_{2'' \text{ plate}}$ psi	10	3.7	139
$E_{1.3''}$ psi	7.2	2.6	112

Since the width of the loading plates in the borehole jack is about 1.3 inches, $E_{1.3"}$, which is the comparable value, was interpolated from the above data. This $E_{1.3"}$ was plotted as a function of e_{ave} in Figure 3-11. Both the borehole jack tests and the plate load tests reveal a very similar behavior. For a void ratio of 0.75, we have the following numerical values:

$$E_{borehole\ jack} = 56\ psi,\ \sigma_v = 0.13\ psi$$

$$E_{plate\ load} = 37\ psi,\ \sigma_v = 0.05\ psi.$$

The difference is not surprising because the confining pressures were not exactly the same and the stress states and deformation modes were different.

The deformation modulus, E, was also plotted on log-log paper as a function of the vertical pressure. This relationship is shown in Figure 3-12. The solid line is drawn through points representing average E from determinations at that particular vertical pressure. The dashed line is for e = 0.75 from Figure 3-11. The equations of the lines in Figure 3-12 can be expressed as:

Average of all data (solid line)

$$E = 51 \times \sigma_v^{0.50} \quad . \tag{3-2}$$

At constant void ratio, e = 0.75

$$E = 77 \times \sigma_v^{0.30} \quad . \tag{3-3}$$

Similar relationships have been found by Kondner and Zelasko, 1963; Duncan and Chang, 1969; Kulhany and Duncan, 1970; and Houston, Namiq, Mitchell, and Treadwell, 1970 (see Vol. I, Chapter 1). The equation for the relationship presented by Houston, Namiq, Mitchell, and Treadwell, 1970, for e = 0.80, and the same LSS No. 2 is

$$E_i = 30\ \sigma_{3f}^{0.45} \quad . \tag{3-4}$$

The above comparisons demonstrate the potential usefulness of the borehole jack technique for the determination of lunar soil properties in situ.
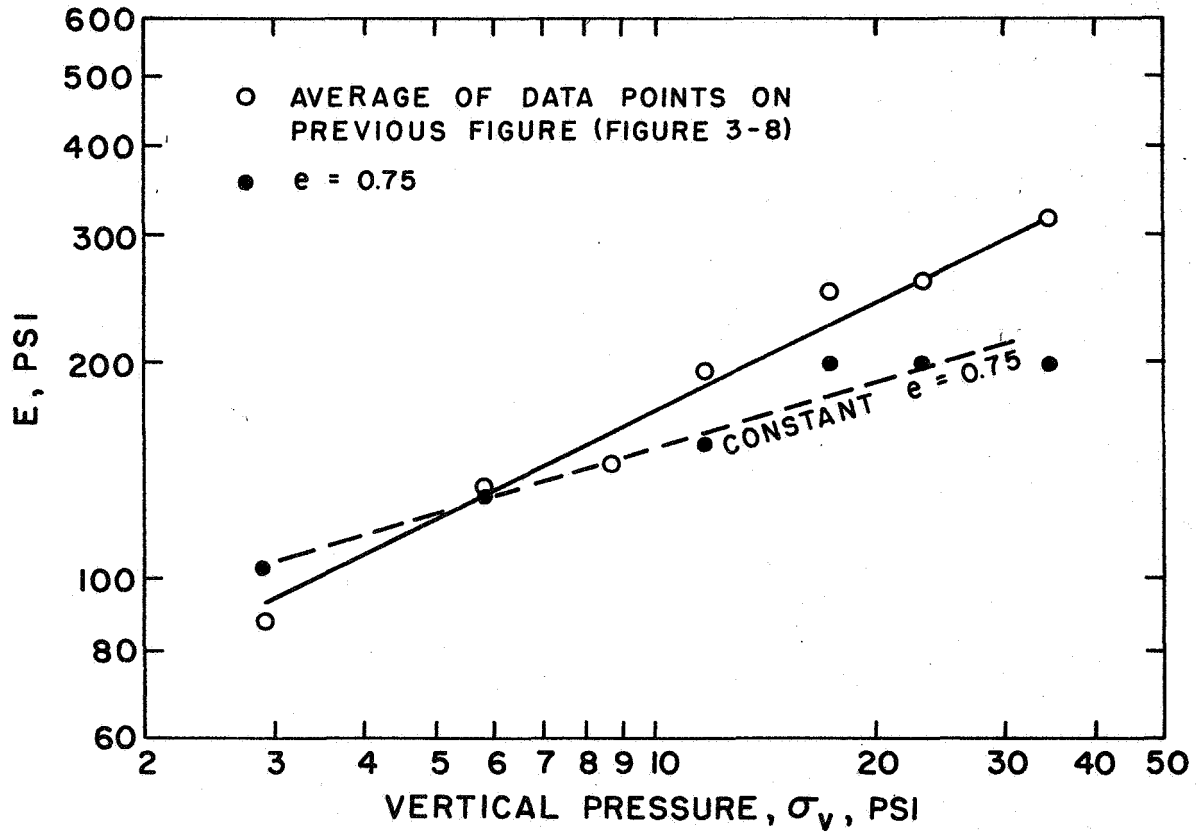
Fig. 3-12. Deformation modulus vs. σ_v.

CONCLUSIONS AND RECOMMENDATIONS

Conclusions:

1. The results are encouraging, considering that this was essentially a first experiment.

2. The borehole jack and associated testing technique can yield valuable soil data.

3. Provided some additional testing in simulated lunar soil and some improvements in the equipment are undertaken, the borehole jack or a similar device could be used to estimate properties of the lunar regolith. This would be possible by comparing the curve obtained in situ on the moon with curves obtained from experimenting with the LSS No. 2. On such a basis, one could estimate in situ soil density and void ratio.

Recommendations:

1. Since the pressure required to expand the jack in soil is considerably less than the design capacity of the jack, it may be desirable to design a much smaller and lighter device for actual lunar use. (The weight of equipment that can be taken to the moon is and will be a limiting factor.)

2. Should such a device be adopted for actual lunar use, additional experimentation would be required and emphasis should be placed on obtaining more precise relationships.

3-22

REFERENCES

Duncan, J. M., and Chang, C-Y (1969), "Nonlinear Analysis of Stress and Strain in Soils," submitted to *ASCE* for publication, 1969.

Egorov, K. E., "Concerning the Question of the Deformation of Bases of Finite Thickness," Mekhanika Gruntov, Sb. Tr., No. 34, Gosstroiizdat, Moscow, 1958.

Harr, M. E., *Foundations of Theoretical Soil Mechanics*, McGraw-Hill Book Co., New York, 1966.

Houston, W. N., Namiq, L. I., Mitchell, J. K., and Treadwell, D. D. (1970), "Lunar Soil Simulant Studies," Final Report: Vol. I, Chapt. 1.

Kondner, R. L., and Zelasko, J. S. (1963), "A Hyperbolic Stress-Strain Formulation for Sands," *Proc. Second Pan-American Conf. Soil Mechanics & Foundation Engr.*, Vol. 1, Rio de Janeiro, 1963, pp. 289-324.

Kulhawy, F. H., and Duncan, J. M. (1970), "Nonlinear Finite Element Analysis of Stresses and Movements in Oroville Dam," Geotechnical Engineering Res. Report, Depart. Civil Engr., University of California, Berkeley.

Terzaghi, K., *Theoretical Soil Mechanics*, John Wiley & Sons, Inc., New York, 1943.

University of California, Dept. of Civil Engineering - Institute of Transportation and Traffic Engineering, *Stresses and Deflections in Foundations and Pavements*, Berkeley, 1965.

APPENDIX

Machine Drawings of Lunar Borehole Jack

ITEM No	QUANTITY	Drawing No	ITEM No	QUANTITY	DESCRIPTION
1	1	C-64-0-1	16	3	No 62270S "O" Ring Rubber
2	1	C-64-0-2	17	56	No 62270A
3	2		18	6	No 62271-A
4	3	C-64-0-3	19	2	No Dix 4612-55 Thomson Ball Bushing
5	2		20	2	No JSC Miniature Precision Ball/Precision Air Coil, NH
6	24		21	2	5mm, No 18-1301 Steel Music Wire, 18 Active Coils with Inactive End Coils, 25 Free Length Ground Ends
7	2		22	2	No 400 DC-A Schaevitz LVDT
8	3		23	2	Core
9	2		24	12	No 0-80 1/4 lg F.H.M.S Steel
10	2		25	4	No 3-48 - 1/2 lg
11	2		26	12	No 5-40 1/4 lg
12	2		27	4	No 1-72 1/4 lg Fillister Hd Scr. Steel
13	2	C-64-0-4	28	4	No 4-40 1/16 lg Allen Hd Scr. Steel
14	2		29	12	No 4-40 3/8 lg
15	1		30	6	No 6-32 11/4 lg
			31	3	1/2 Thick Gasket Rubber
			32	2	No 4-40 Nuts, Steel

SECTION E-E

SECTION D-D

SECTION C-C

SECTION B-B

SECTION A-A

scale

0 1" 2" 3"

Fig. 3-A1. Lunar borehole jack assembly.

Fig. 3-A2. Lunar borehole jack, internal details.

Fig. 3-A3. Lunar borehole jack, external details.

Fig. 3-A4. Lunar borehole jack, piston details.

TYPE 304 STAINLESS STEEL

COLD DRAWN SCREW STOCK STEEL

17			
13	2		
14	2		
15	1		

#53(.0595)DRILL, 0.51 DEEP
#1-72 NF5 TAP, 6 HOLES
ON 0.75 DIA. B.C., 60° APART

#43(.089)DRILL
#4-40 NC2 TAP.
2 HOLES

DRILL, C'BORE
FOR NO. 4 ALLEN HD. SCR.
2 HOLES

SECTION A-A

.90 DIA

3.50

2.0

.88

.56

.562 DIA

.25 DIA

.6

3.25

.75
.16
.50
.12
.151 DIA

(14)

#43(.089)DRILL, #4-40 NC2 TAP

SECTION A-A

.61
.94
.06
.94
.34
.18

.62 DIA

.560 DIA

2.75

.62

.17
.12

.561 DIA
.90 DIA

0.06 × 45° CH.

DRILL, 6 HOLES
60° APART ON 0.75 DIA. B.C.

0.25 × 45° CHAMF.

.75

.5000 DIA

1.25

.250 DIA

.406 DIA

.19
.16

.28
.266
.422
.031
.250
.250
.60

DRILL, 3 HOLES

(13)

½-18 CLASS 2 T-DS
BOTH ENDS

.6
2.50
4.58
.28 DIA
12.0
.6
.31 DIA

(15)

scale: 1" = 2"

LUNAR BORE HOLE JACK

DRAWN BY R.
REVIS.

DATE: 2-27-70

COLLEGE OF ENG.
UNIVERSITY OF CALIFORNIA

Fig. 3-A5. Lunar borehole jack, LVDT details.